8

NASA CR- 147456
ERIM 102300-19-F
E7.6-10192

Final Report

ANALYSIS OF HYDROLOGICAL FEATURES OF PORTIONS OF THE LAKE ONTARIO BASIN USING SKYLAB AND AIRCRAFT DATA

FABIAN C. POLCYN, DIANA L. REBEL,
and JOHN E. COLWELL

Infrared and Optics Division

JANUARY 1976

(E76-10192) ANALYSIS OF HYDROLOGICAL FEATURES OF PORTIONS OF THE LAKE ONTARIO BASIN USING SKYLAB AND AIRCRAFT DATA Final Report, Mar. 1973 - Dec. 1975 (Environmental Research Inst. of Michigan) 100 p HC $5.00 G3/43

N76-18613

Unclas
00192

Prepared for

NATIONAL AERONAUTICS AND SPACE ADMINISTRATION

Johnson Space Center
Houston, Texas 77058
Contract NAS9-13275

ENVIRONMENTAL
RESEARCH INSTITUTE OF MICHIGAN
FORMERLY WILLOW RUN LABORATORIES, THE UNIVERSITY OF MICHIGAN
BOX 618 • ANN ARBOR • MICHIGAN 48107

TECHNICAL REPORT STANDARD TITLE PAGE

1. Report No.	2. Government Accession No.	3. Recipient's Catalog No.
NASA CR-ERIM 102300-19-F		

4. Title and Subtitle	5. Report Date
Analysis of Hydrological Features of Portions of the Lake Ontario Basin using Skylab and Aircraft Data	September 1975
	6. Performing Organization Code

7. Author(s)	8. Performing Organization Report No.
Fabian C. Polcyn, Diana L. Rebel, and John E. Colwell	102300-19-F

9. Performing Organization Name and Address	10. Work Unit No.
Environmental Research Institute of Michigan Infrared and Optics Division P.O. Box 618 Ann Arbor, Michigan 48107 (313) 994-1200	11. Contract or Grant No. NAS9-13275
	13. Type of Report and Period Covered Final Report March 1973 - December 1975
12. Sponsoring Agency Name and Address National Aeronautics and Space Administration Johnson Space Center Houston, Texas 77058	14. Sponsoring Agency Code

15. Supplementary Notes

16. Abstract

The usefulness of Skylab and aircraft data for mapping features of hydrological interest in portions of the Lake Ontario drainage basin has been investigated. S190A and S190B photography are useful for mapping large scale gemorphological features and for assessing water depth and water quality.

The available S192 data was affected by low frequency noise due to a diode light which was inadvertently left on during data collection, but data preparation was successful in partially reducing this problem. The resulting data was processed using a red, near IR, and thermal band to produce a map and areal statistics of hydrologically significant features.

A thermal model and a reflectance model for determination of soil moisture were developed and implemented on aircraft data over a site where field determinations of soil moisture had been made. The reflectance model appears to have promise for inferring surface soil moisture in partially vegetated terrain.

ORIGINAL CONTAINS

COLOR ILLUSTRATIONS

17. Key Words	18. Distribution Statement
Skylab Remote sensing Hydrology Soil moisture Lake Ontario basin IHD	Initial distribution is listed at the end of this document.

19. Security Classif. (of this report)	20. Security Classif. (of this page)	21. No. of Pages	22. Price
Unclassified	Unclassified	ix plus 93	

PREFACE

This report is submitted in fulfillment of National Aeronautics and Space Administration Contract No. NAS9-13275. Mr. Larry York was Technical Monitor for the project. Work at ERIM was performed principally by Diana Rebel and Dr. John E. Colwell, under the direction of Fabian Polcyn, the Principal Investigator.

The purpose of our research was to assess hydrological conditions of selected portions of the Lake Ontario drainage basin. Among the conditions of interest were soil moisture, land use, water quality, and water currents.

Work was done with assistance from personnel at the University of Guelph, Guelph, Ontario Canada. Dr. Richard Protz directed the soil moisture analyses and Dr. Allen Falconer and several of his graduate students assisted in the collection of field data. Rajendra Aggarwala, graduate student at the University of Michigan, assisted in the development of the reflectance soil moisture algorithm. ERIM personnel who contributed to the success of the project included Dr. Robert Horvath, who advised us on the use of his thermal soil moisture model; Peter Lambeck, who helped preprocess the S192 data to remove effects of striping in the data; Bette Salmon, who assisted in collection of field data; Frederick Thomson, who assisted in the solution of problem areas; Dr. William Benjey and John Stinson, who performed the interpretation and analysis of the S190A and S190B photography; and Debbi Compton, who provided valuable secretarial support.

CONTENTS

FIGURES

TABLES

ANALYSIS OF HYDROLOGICAL FEATURES OF PORTIONS OF THE LAKE ONTARIO BASIN USING SKYLAB AND AIRCRAFT DATA

1
INTRODUCTION

The main objective of this Skylab project was to map parameters of hydrological significance in portions of the Lake Ontario drainage basin. This project was intended to supplement information gathered during the International Hydrological Decade (1964-1973).

The Lake Ontario drainage basin is outlined on the ERTS mosaic in Figure 1. The coverage for the S192 data we received is indicated. S190A and S190B photography were available for this area (the S190A coverage is also indicated in Figure 1) and for a pass that went over the Finger Lakes to the southeast. Several of the Representative Drainage Basins selected by Canada for study during the International Hydrological Decade are also shown. The aircraft data which was processed as part of this effort was obtained over the Elora Research Farm, also indicated in Figure 1.

Skylab S190A and S190B photographs were analyzed to determine what features of hydrological significance could be identified. Attention was given to the best wavelength region and resolution for identification of particular features.

Skylab S192 data were processed to determine what hydrological features could be mapped. Emphasis was placed on identification of terrain classes, since preliminary analysis showed very little variability in the characteristics of the portion of Lake Ontario for which we had data.

The focus of the aircraft data processing effort was on the estimation of soil moisture. The effort was supported by ancillary field data collected by both Canadian and ERIM teams. Both day and

FIGURE 1. LANDSAT-1 MOSAIC OF THE LAKE ONTARIO DRAINAGE BASIN. The outline of the basin is indicated by the solid white line. Coverage of Skylab S192 data from SL3 Pass 29 on September 1973 which we received is indicated by the broken black line. Coverage of the two cloud free frames of S190A photography from the same pass is indicated by the white dashed line. Several IHD representative basins are also indicated: A, East and Middle Oakville Creeks; B, Bowmanville, Wilmot, and Soper Creeks; and C, Moira River. D indicates the Finger Lakes region in New York State. E designates the University of Guelph Research Farm near Elora, Ontario.

night aircraft missions were flown, in order to assess the usefulness of diurnal thermal information for estimation of soil moisture. Modeling of the thermal characteristics of soils as a function of soil moisture was performed in order to assist in the processing and analysis of the aircraft day/night thermal data.

A model for assessing surface soil moisture under variably vegetated terrain using red and reflective IR data was developed. The results of the modeling were used to process the aircraft daytime scanner data in the appropriate spectral bands.

The major conclusions of this project are:

1) S190A and S190B photography are useful for mapping features of hydrological interest, and for assessing water depth and water quality;

2) despite the fact that classification accuracy of the processed S192 data for this project was degraded by a striping noise problem, areal statistics for features of hydrological significance are obtainable from this type of satellite data and would appear to be useful for characterizing large areas;

3) reflectance data in the red and near IR spectral regions show promise for inferring surface soil moisture in partially vegetated terrain.

2

PHOTOINTERPRETATION OF S190A AND S190B PHOTOGRAPHY

Photography from two Skylab overpasses of the Lake Ontario basin was made available to us for interpretation. The specific kinds of imagery we obtained are listed in Table 1.

The following discussion describes our analysis of the available photography. The purpose of this analysis was to determine which features of hydrologic interest can be detected on which types of imagery. We used 2X and 4X enlargements of the positive transparencies and 10X magnification for evaluation and interpretation.

2.1 SL3 PASS 29, 9 SEPTEMBER 1973

2.1.1 STANDING WATER

Land/water boundaries can generally be well located on the Skylab photography, especially in the 0.8 - 0.9 μm band of the S190A package. In this band water has a very high absorptance and thus looks dark, while vegetation and other terrain and cultural features have relatively high reflectance and therefore appear relatively light in tone on positive transparencies or prints. Due to the high contrast between open water and other features even the many very small water bodies, illustrated in Figure 2, show up clearly. One of the disadvantages of the 0.8 - 0.9 μm photography for locating very small water bodies is its relatively coarser resolution than that which is available in the visible bands. In addition, water bodies which are partially covered by vegetation may not be detectable in the 0.8 - 0.9 μm band because of the relatively high IR reflectance of vegetation.

2.1.2 WETLAND AREAS

Wetland areas can be more easily interpreted using color and color IR photography than using one or the other separately. Almost all

TABLE 1

S190A AND S190B PHOTOGRAPHY RECEIVED FROM NASA

SL3 PASS 29, 9 SEPTEMBER 1973

	λ(μm)		Roll No.	Format
				(positive transparencies of all; negative transparencies of the black and white)
S190A	0.5-0.6	Pan X B&W	42	70mm
	0.6-0.7	Pan X B&W	41	4X enlargements
	0.7-0.8	B&W IR	37	
	0.8-0.9	B&W IR	38	
	0.4-0.7	Color	40	
	0.5-.88	Color IR	39	
S190B	0.5-0.7	B&W	85	4.5 inches 2X enlargements

SL3 PASS 50, 19 SEPTEMBER 1973

S190A	0.5-0.6	Pan X B&W	48	70mm
	0.6-0.7	Pan X B&W	47	4X enlargements
	0.7-0.8	B&W IR	43	
	0.8-0.9	B&W IR	44	
	0.4-0.7	Color	46	
	0.5-.88	Color IR	45	
S190B	0.4-0.7	Color	88	2X enlargements

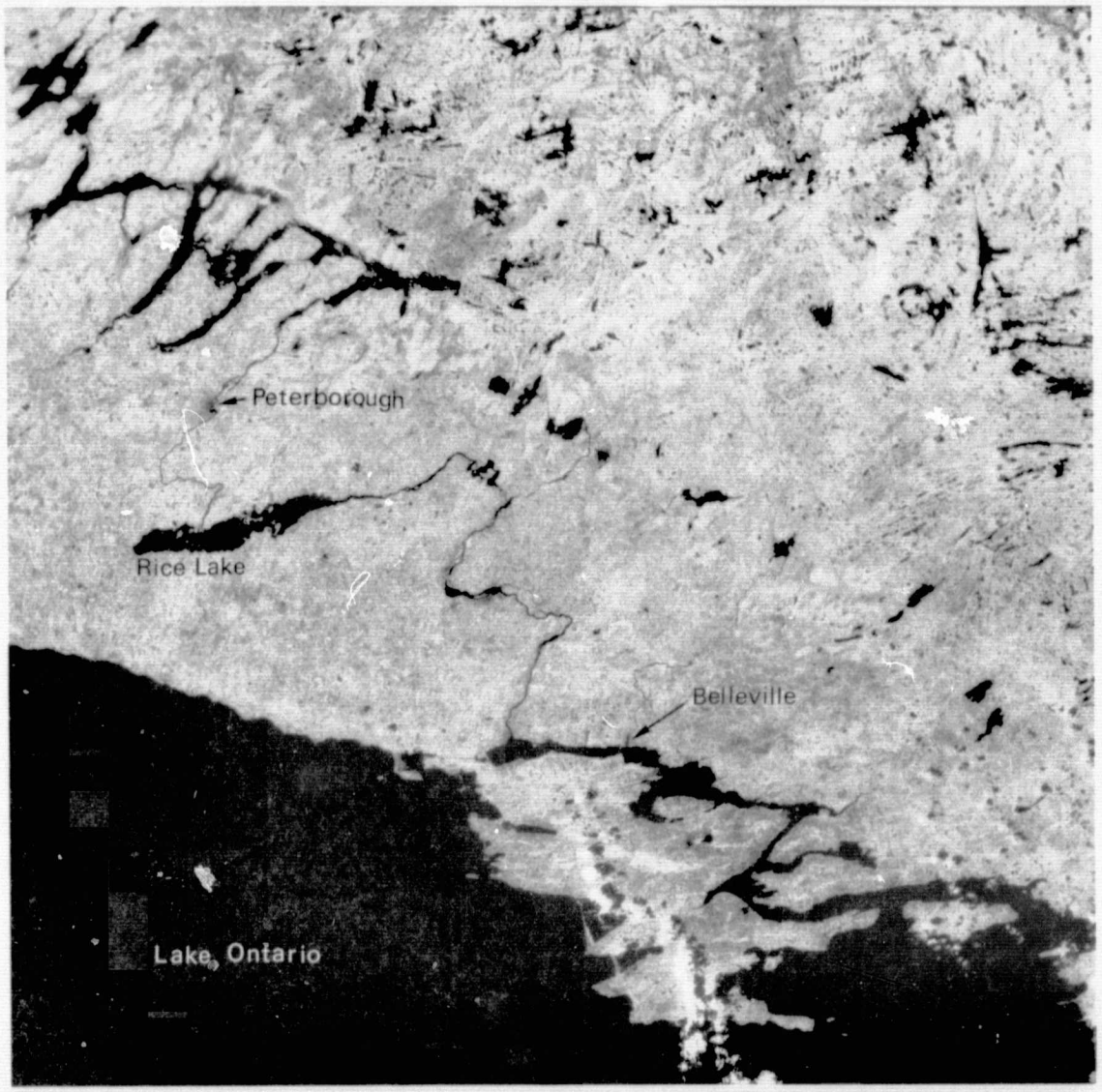

SL3 Pass 29
Roll 38 Frame 17

5 0 20 mi
5 0 30 km
Scale

N

FIGURE 2. BLACK AND WHITE S190A PHOTOGRAPH (0.8-0.9 μm) OBTAINED 9 SEPTEMBER 1973 OVER A PORTION OF SOUTHEASTERN ONTARIO PROVINCE, CANADA.
Note the numerous small lakes which appear dark on this infrared image.

water bodies and wetlands show up dark on the color film. Using color IR imagery one can detect vegetation because of the reddish tones produced by the relatively high green and IR reflectance of the vegetation. The information from the two kinds of imagery thus make it possible to detect those wetlands that have floating vegetation, emergent vegetation, or standing vegetation (trees and shrubs) (Figures 3 and 4). Using the S190B (Earth Terrain Camera) one can make this separation using just the 0.5 - 0.7 μm black and white band, although with greater difficulty (Figure 5). Perhaps the finer resolution of the S190B allows the separation to be made by detecting more texture in the vegetated areas.

2.1.3 WATER DEPTH, WATER QUALITY, AND WATER CURRENTS

Shallow water depths can generally be detected using S190A photography, especially when the bottom material is sandy and/or light-toned. Due to the relatively high transmittance of the visible wavelengths, shallow water areas frequently show up light blue in both color and color IR photography. Near shore regions of a shallow sandy-bottomed lake may appear almost white. Such is the case near Outlet Beach Provincial Park looking out into Athol Bay (Figures 3 and 4). A ground photo of this area taken by ERIM investigators (Figure 3) shows a rather flat, sandy beach, and on the Skylab photography one can see apparent effects of the lake bottom up to 1/2 mile offshore. Another example of this phenomenon occurs in Sandy Lake, about 14 miles north of Peterborough (Figures 3 and 4).

Suspended solids show up best in the 0.5 - 0.6 μm band and in the 0.4 - 0.7 μm (S190A) color photography. If there is no variation in the light tone over wide areas, one can reasonably assume the cause to be a uniform amount of suspended solids rather than bottom effects, in that the water depth would be expected to vary if there were variations in the bottom topography. An example of this phenomenon can be seen in the north-east part of Lake Scugog (Figure 6).

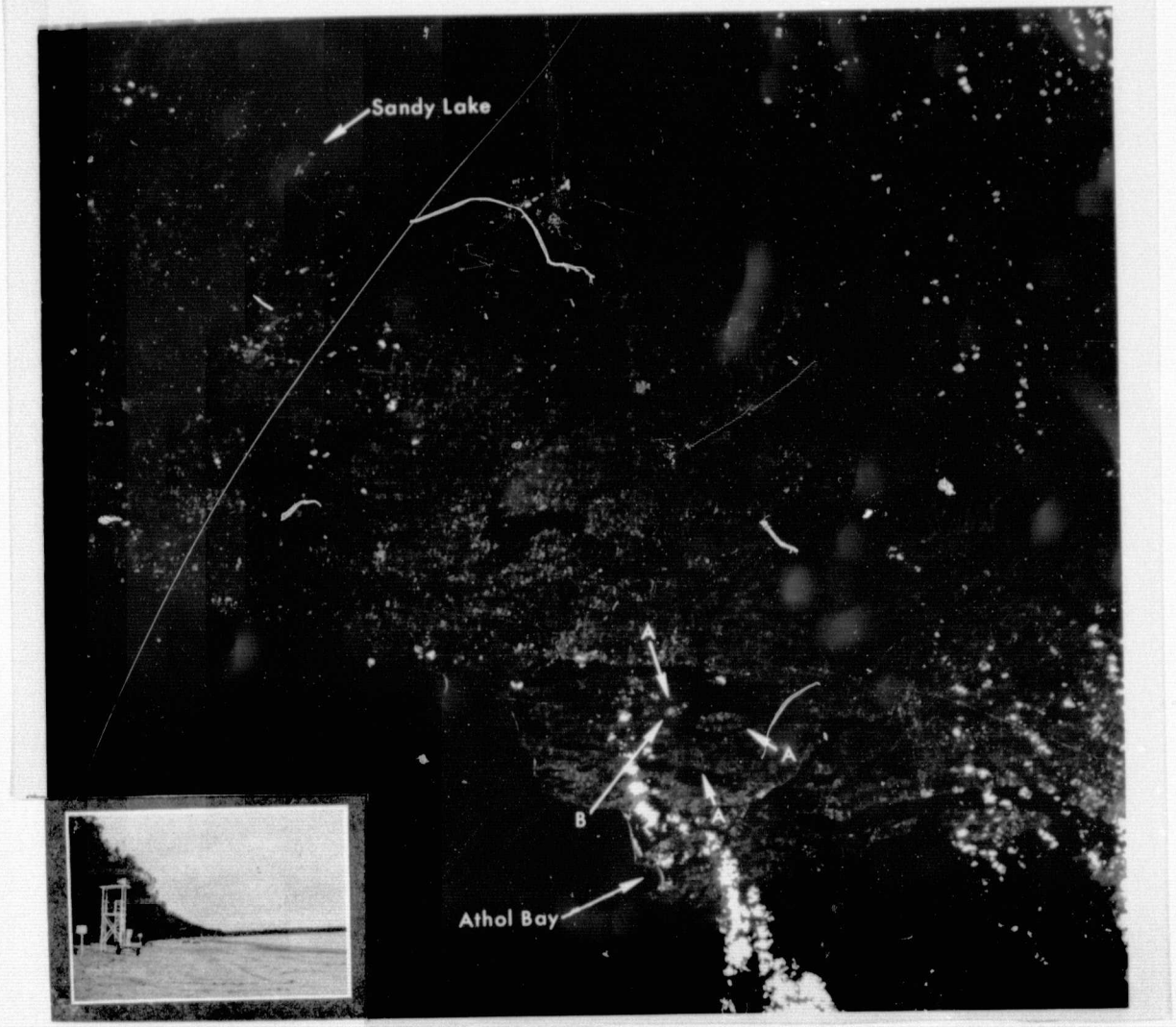

FIGURE 3. COLOR S190A PHOTOGRAPH OBTAINED 9 SEPTEMBER 1973 OVER A PORTION OF SOUTHEASTERN ONTARIO PROVINCE, CANADA. A designates extensive areas of cattails (Typha spp.), B designates swamp areas of mixed conifer and deciduous tree species. Compare these areas with their counterparts in Figures 2 and 4. Inset is a black and white print of a color transparency taken 13 September 1973 looking out into Athol Bay from Outlet Beach Provincial Park.

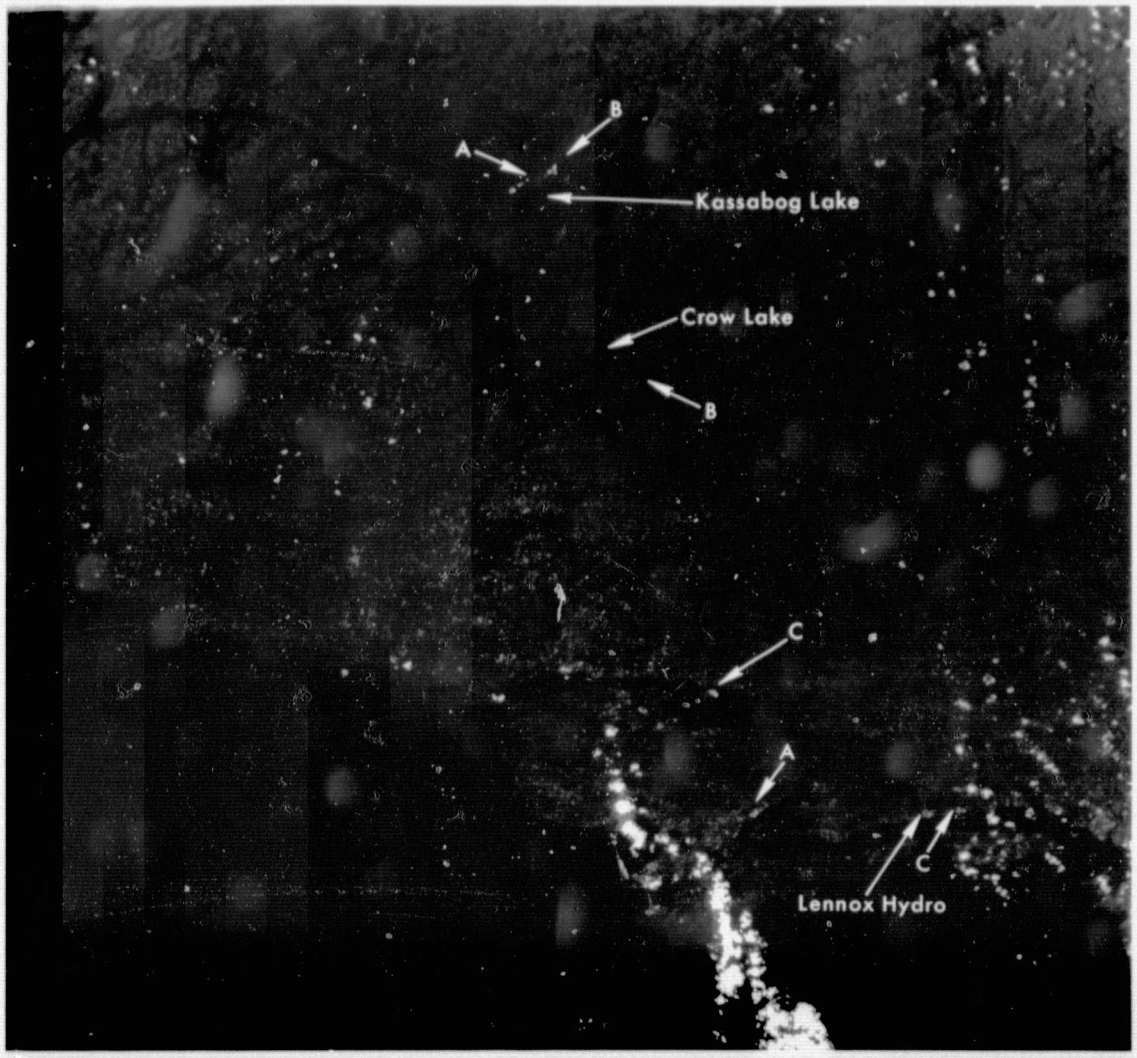

SL3 Pass 29
Roll 39 Frame 17

5 0 20 mi

5 0 30 km

Scale

N

FIGURE 4. COLOR IR S190A PHOTOGRAPH OBTAINED 9 SEPTEMBER 1973 OVER A PORTION OF SOUTHEASTERN ONTARIO PROVINCE, CANADA. Compare with Figure 3. A indicates quarries, B open pit mining operations, and C cement plants.

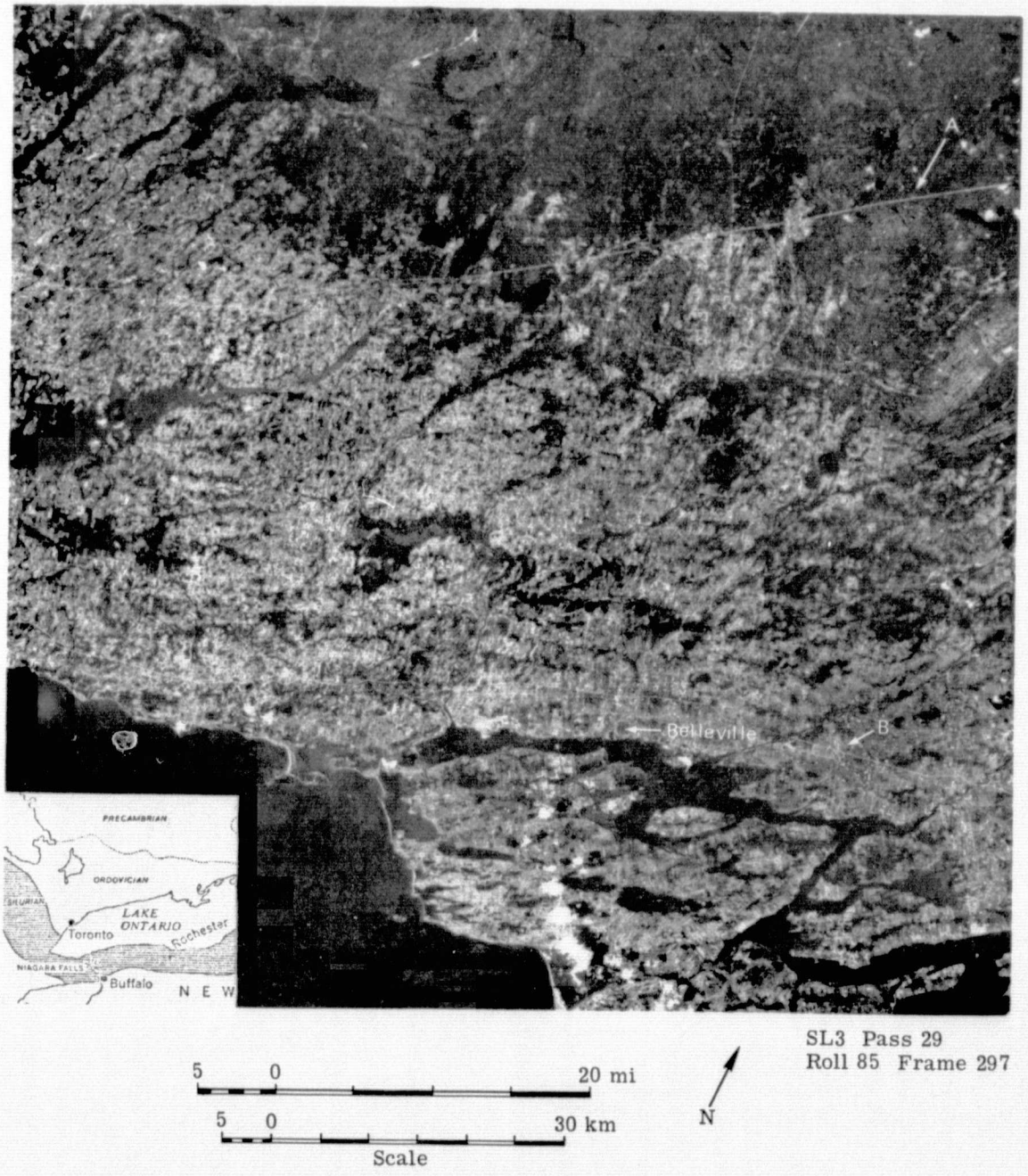

FIGURE 5. BLACK AND WHITE S190B PHOTOGRAPH (0.5-0.7 μm) OBTAINED 9 SEPTEMBER 1973 OVER A PORTION OF SOUTHEASTERN ONTARIO PROVINCE, CANADA. Compare the marsh and swamp areas indicated on Figure 3 with the corresponding areas on this image. A indicates powerline right of way, B indicates Highway 401. Inset shows the gross geologic structure of the bedrock.

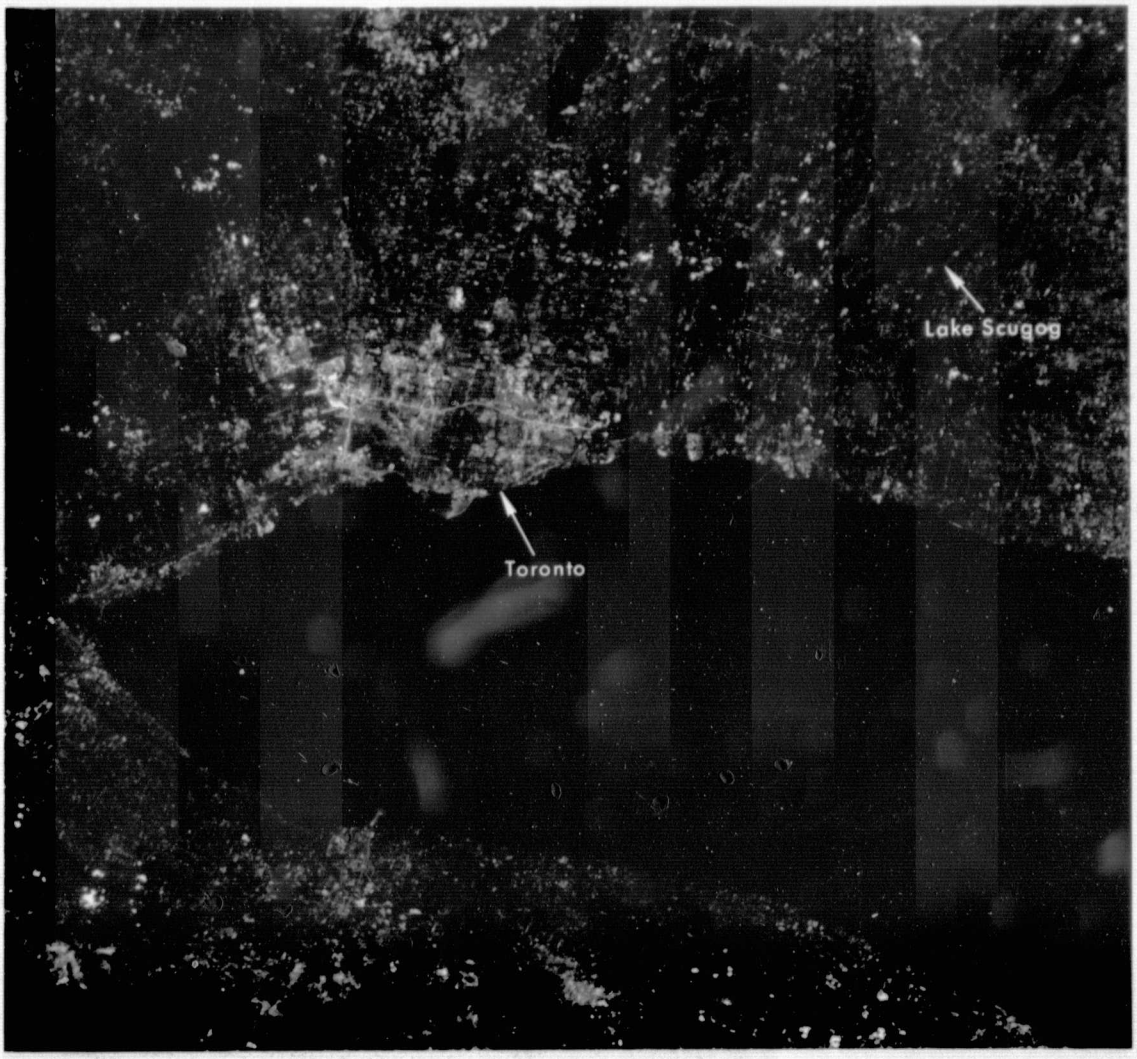

FIGURE 6. COLOR S190A PHOTOGRAPH OBTAINED 9 SEPTEMBER 1973 OVER WESTERN LAKE ONTARIO

Irregular suspended sediment patterns are frequently a good indicator of currents. An example of this can be seen on the 0.5 - 0.6 μm band (S190A) image of Lake Ontario (Figure 7). The patterns seen roughly correspond to current patterns predicted for westerly wind conditions (which are known to have prevailed at the time) in a model by Bonham-Carter and Thomas [1], and sediment transport patterns for the prevailing conditions, as modeled by Simons [2]. The westerly coastal jet currents are revealed by the eastward deflection of the plumes from the Niagara River, Welland Canal, Port Dalhousie, and Toronto Harbor.

Differences in the character of these plumes can also be detected. For example, the Niagara plume is composed of relatively dark water, and is apparent by its contrast to the surrounding more reflective plumes. The reason for the difference is unknown.

2.1.4 TERRAIN FEATURES

Using the S190A and S190B photography one can observe large geological/geomorphological and cultural features in a single frame. Evidence of glacial influence on the northern shore of Lake Ontario can be seen in several areas. Most striking is the boundary, running approximately East--West, between the Ordovician and Precambrian bedrock areas (Figures 3, 4, and 5). Glacial scouring lines, which are evidence of the removal of the sedimentary deposits and exposure of the crystalline Precambrian rocks, are evident. The soil in this area is basically poor and shallow and little farming is done. The area is covered by natural vegetation, principally forest, which further accentuates the appearance of the division between the Precambrian and the Ordovician to the south. The limestone rich Ordovician has produced good soils and this area is characterized by few remaining expenses of forest and many farmed areas.

Urban and built up areas are seen best using the 0.5 - 0.6 μm and 0.6 - 0.7 μm regions combined; thus, color photography is useful in this

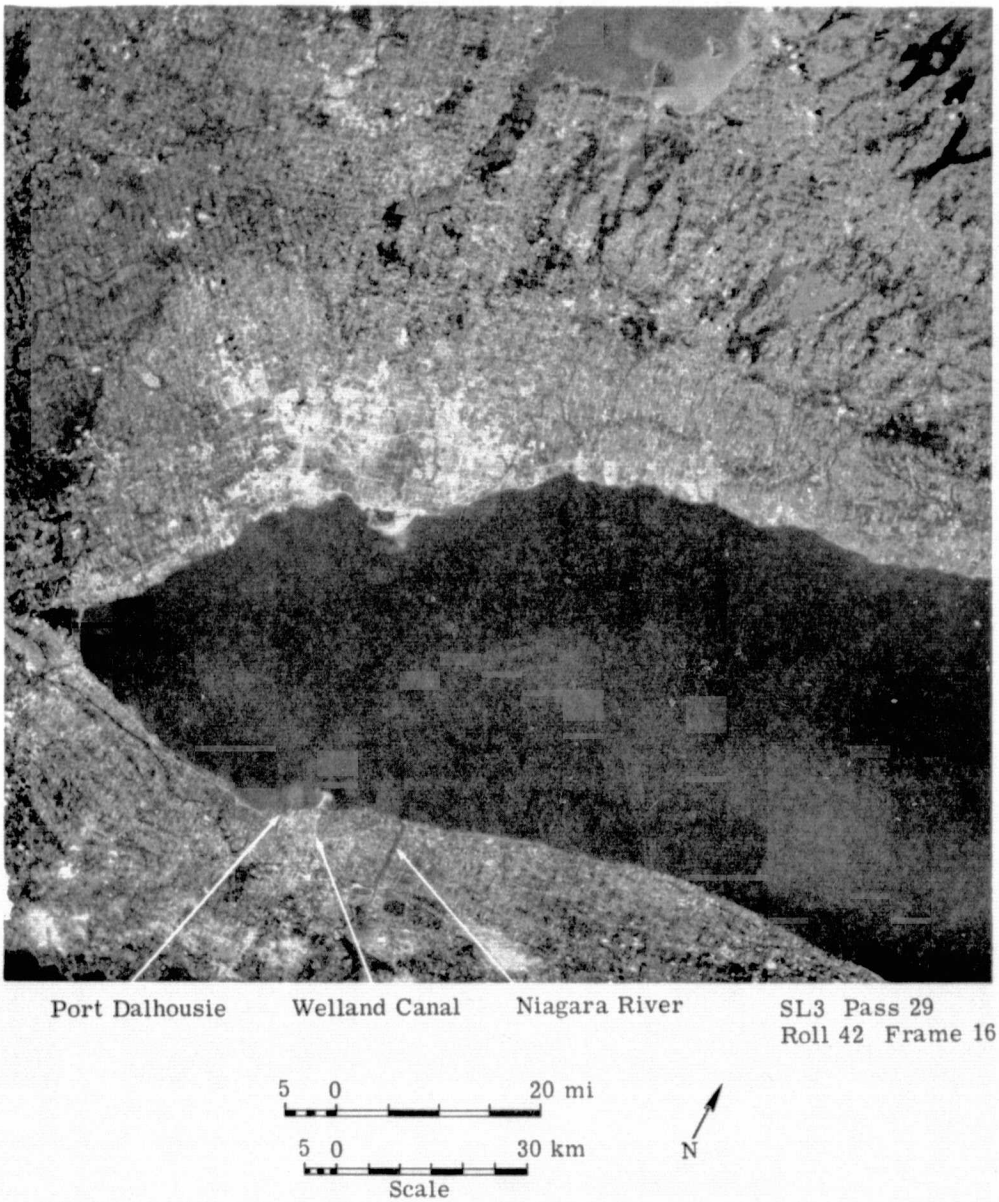

FIGURE 7. BLACK AND WHITE S190A PHOTOGRAPH (0.5-0.6 μm) OBTAINED 9 SEPTEMBER 1973 OVER WESTERN LAKE ONTARIO. Note the current patterns in Lake Ontario indicated by the irregular distribution of suspended solids.

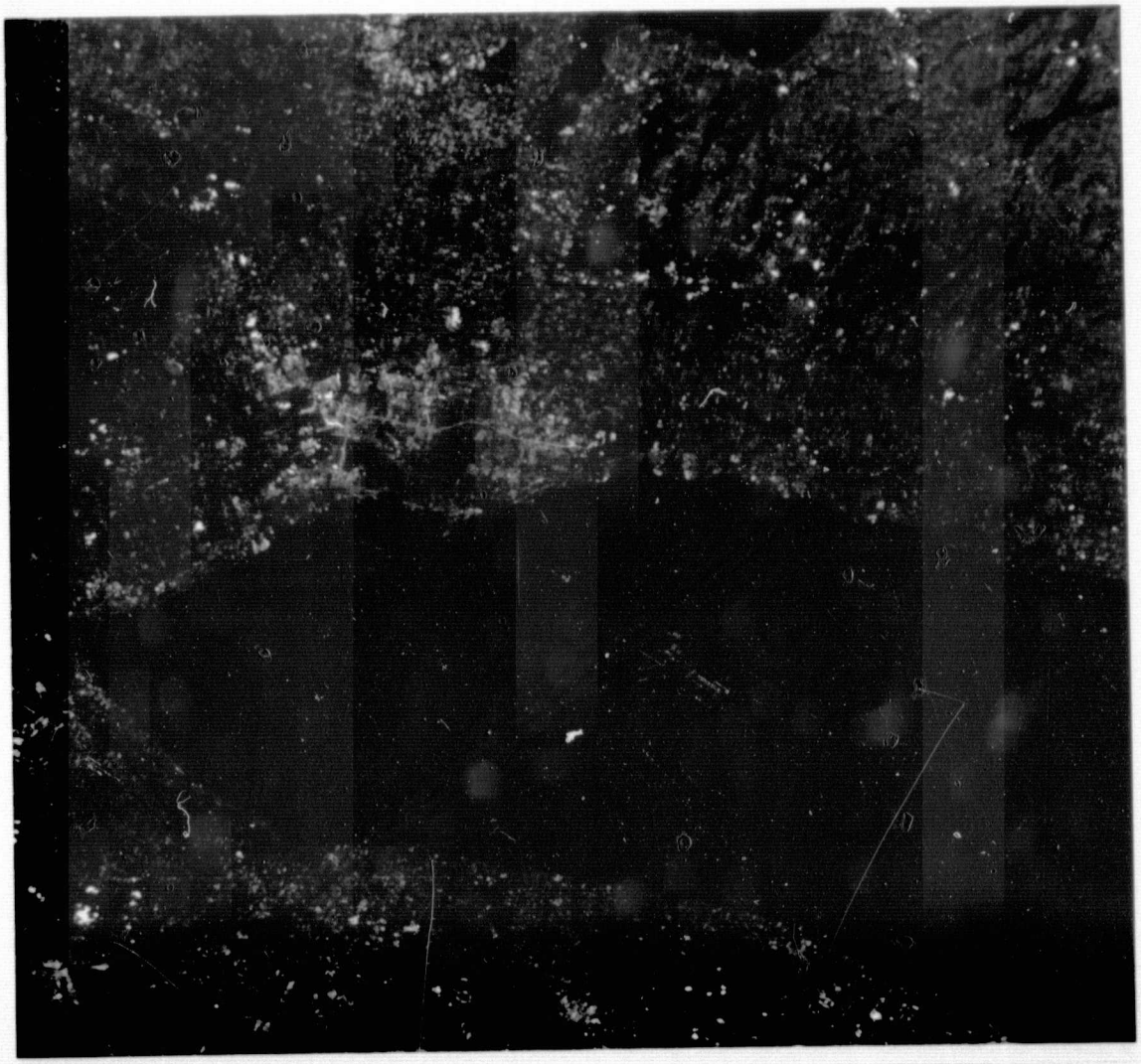

FIGURE 8. COLOR IR S190A PHOTOGRAPH OBTAINED 9 SEPTEMBER 1973 OVER WESTERN LAKE ONTARIO

type of interpretation. In color imagery the heavily built up areas will be light in color due to the concrete, roofing material, and bare ground (Figures 3 and 6). Color IR photography is also useful in delineating urban areas. Here the urban areas are light blue in color while the vegetation shows up red to give good contrast between vegetated and urban areas (Figures 4 and 8). Open pit mining operations and quarries can also be seen as very light in color. For example, in Figure 4 one mine is just northeast of Kasshabog Lake and another, with extensive tailing piles, is just southeast of Crowe Lake.

Using the Earth Terrain camera (S190B) one can distinguish such detailed features as residential streets, for example, in the town of Belleville (Figure 5). In addition, in many areas the median of Highway 401 can be clearly seen. Transmission line right-of-ways can easily be separated from roads by observing the width difference, tonal difference, and the edge sharpness in the linear feature.

Color IR film can also be used in conjunction with normal color film to identify right-of-ways. On color film roads and transmission line right-of-ways show up well, but on color IR imagery the right-of-ways show up very poorly. This is because the right-of-ways are covered by grass and short vegetation, and the area through which the right-of-way was cut is covered by trees and brush, all of which have a similar appearance on the color IR imagery.

2.2 SL3 PASS 50, 19 SEPTEMBER 1973

Although some of this area was covered by high cirrus clouds which prevented effective computer processing, some photointerpretation of the area was possible. In general, the same kinds of information can be obtained from this pass as were obtained from Pass 29.

For example, the south end of Otisco Lake appears light in tone in the (S190A) 0.5-0.6 μm photography and the 0.6 - 0.7 μm photography, as well as in the color photography (Figure 9). This would indicate a

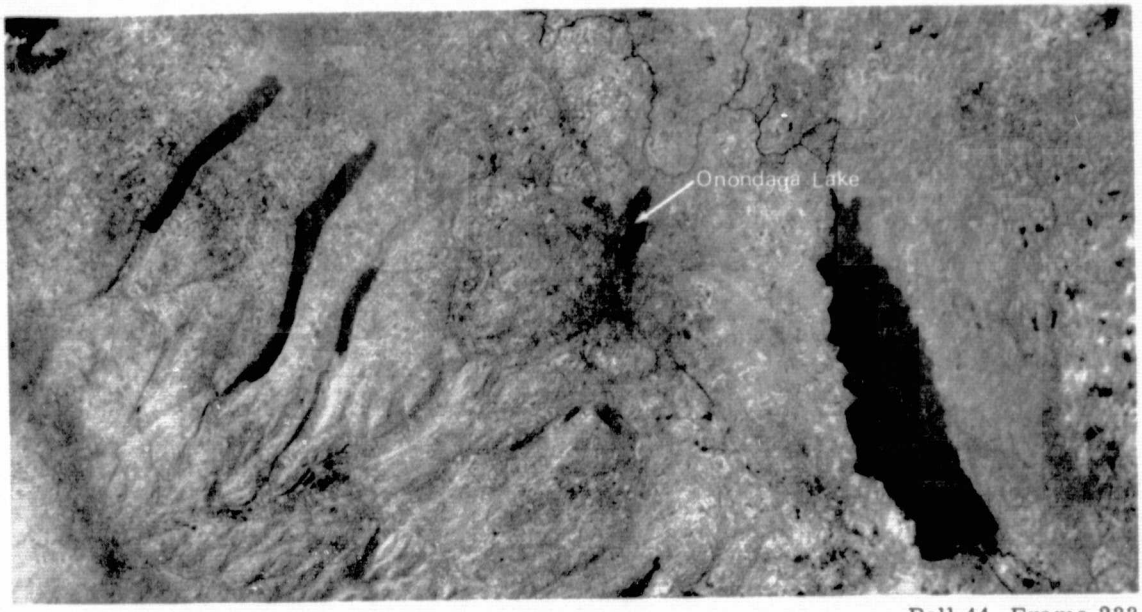

(a) 0.8-0.9 μm

Roll 44 Frame 233

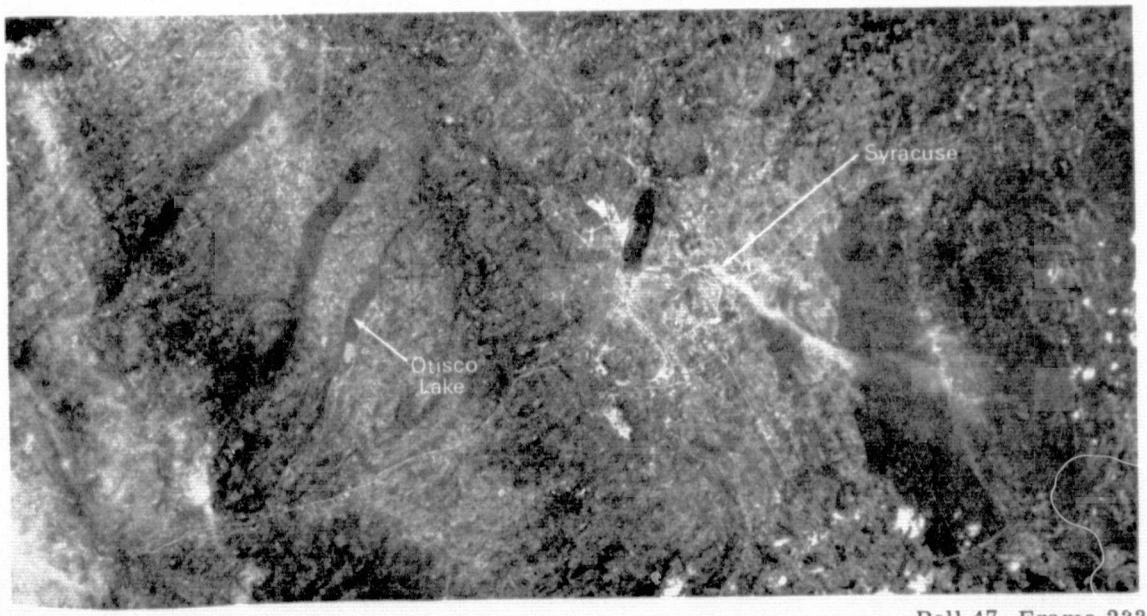

(b) 0.6-0.7 μm

Roll 47 Frame 233

5 0 20 mi

5 0 30 km

Scale

N

FIGURE 9. PORTION OF S190A PHOTOGRAPHS OBTAINED 19 SEPTEMBER 1973 DURING SL3 PASS 50 OVER THE FINGER LAKES AREA, NEW YORK STATE

uniformly very shallow area or an area with a large amount of suspended sediments. In the IR photography (Figure 9) the area appears dark toned, but not as dark toned as the north end of the lake. This slightly lighter tone suggests that the area may have little or no standing water (e.g., mud flats) and/or it may have a small amount of vegetation growing on it.

Using S190A and S190B photography one can see a cloudiness in the south end of Onondaga Lake. This cloudiness is apparently due to suspended sediments coming from a discharge point. The phenomenon shows up as well on 0.6 - 0.7 μm photography as on 0.5 - 0.6 μm photography. This fact suggests that the composition of this sediment may be different from that which showed up best in the 0.5 - 0.6 μm band elsewhere, or that the sediment is located nearer the surface.

2.3 CONCLUSIONS

In conclusion, a number of features of hydrological interest can be interpreted on S190A and S190B photography. Different kinds of features are best distinguishable in different spectral bands (or color combinations) from the green to the near IR. The S190B photography suggests that the best possible resolution will lead to the most accurate identification of some features. Therefore, we believe that the optimum camera array for hydrologic analyses would be multispectral and would have high resolution.

For those users who do not have access to automatic data processing capabilities the use of S190A and S190B photography appears to show considerable promise for analyzing large drainage basins.

Table 1-A summarizes our analysis of the capabilities of S190A and S190B photography for assessing conditions of hydrologic significance in the Lake Ontario basin.

TABLE 1-A

SUMMARY OF THE USEFULNESS OF S190A AND S190B PHOTOGRAPHY FOR ASSESSING CONDITIONS OF HYDROLOGIC SIGNIFICANCE. Analysis is based on the imagery we received. Checks indicate imagery found to be most useful for analysis of various features.

	S190A						S190B	
Feature of Interest	.5-.6 μm	.6-.7 μm	.7-.8 μm	.8-.9 μm	.4-.7 μm (color)	.5-.88 μm (color IR)	.4-.7 μm (color)	.5-.7 μm (B&W)
Standing Water			✓	✓				
Wetlands					✓	✓		✓
Water Depth					✓	✓		
Water Quality	✓				✓			
Water Currents	✓							
Urban Features	✓	✓			✓	✓	✓	✓

3
AIRCRAFT PROCESSING IN SUPPORT OF SKYLAB DATA

One of the main objectives in this project was to apply Skylab data to measure hydrological parameters of importance. Soil moisture has been one parameter of considerable importance in the hydrological cycle and in the management of water resources.

If a method could be developed to measure soil moisture over an entire watershed by extending soil moisture point samples then a major contribution would have been achieved. It is too costly and cumbersome to try to measure soil moisture for a large number of points.

The plan was to use aircraft data of high spatial resolution as the link between ground measurements and the relatively coarse resolution of Skylab data. The ERIM M7 multispectral scanner records data in spectral bands similar to the Skylab S192 data, and therefore is a low altitude analog of S192. Simultaneous flights over the same area by the ERIM M7 and the Skylab S192 were planned in an attempt to extrapolate results from aircraft data to results from space data.

However, S192 data were not obtained over the area where ground data were available. Consequently, we considered using aircraft indications of soil moisture as "ground data" for investigating the feasibility of using S192 data for estimating soil moisture in areas where aircraft and Skylab data were coincident. However, the distortions due to the conic format of the S192 data made it difficult to locate identical areas on the two types of data. The small size of fields in the area provided additional complications, and suggested that processing of S192 data for soil moisture would have been extremely difficult, at best. Emphasis was thus placed on processing of the aircraft data, so that the concurrent field data which was collected could be utilized. This section describes how the aircraft data was processed.

Two methods for estimating soil moisture were tested, one based on thermal data and one based on data in red and near IR spectral bands. The method using thermal data proved inconclusive, but the method using red and near IR spectral bands shows promise. Such a method might be applied to very large areas by using data with spectral bands similar to those found in the Skylab S192 package.

3.1 DATA COLLECTION

3.1.1 AIRCRAFT COVERAGE

Two underflights for Skylab were flown by the ERIM C-47 aircraft over test sites located on the Canadian shore of Lake Ontario on 10 and 11 September 1973. A total of 144 nautical miles was flown over four sites on 10 September. On 11 September only one site was flown. Multispectral data from the ERIM M7 scanner and aerial photographic data were obtained on 10 September 1973. Only thermal data were collected during the pre-dawn flight on 11 September due to the low light level. Table 2 is a brief summary of the flights. Refer to reference 16 for details. Several test sites previously flown under the ERTS program and others were chosen in order to allow for the shifting ground track of Skylab.

Conditions during the day mission (all ten flightlines) were excellent, with no cloud cover and greater than 18 miles visibility. The following morning, however, there was a heavy overcast with visibility less than five miles. Scheduled flight altitude was 5,000 ft above the ground but the aircraft flew below the cloud ceiling until conditions forced the flight to be aborted. While some useful data was obtained, coverage did not coincide with that obtained during the day flight as much as had been intended.

3.1.2 GROUND DATA COLLECTION

Concurrent with the daytime and pre-dawn aircraft flights over the Guelph area, personnel from the University of Guelph collected soil

TABLE 2

SUMMARY OF ERIM C-47 AIRCRAFT COVERAGE OVER FOUR SITES
IN ONTARIO, CANADA ON 10 AND 11 SEPTEMBER 1973

Date	Area	Altitude Above Terrain (ft)	Time (Local) Start - Stop		Number of Flightlines	Total Nautical Miles Flown
10 Sept	Guelph	5000	1317	1335	2	24
10 Sept	Oakville River Basin	6000	1341	1411	3	48
10 Sept	Bowmanville River Basin	8000	1432	1450	3	24
10 Sept	Moira River Basin (Belleville)	8000	1511	1537	2	48
11 Sept	Guelph	2500/1000	0632	0654	3	42

samples which were later analyzed for moisture content and bulk density. At the time of the pre-dawn flight ERIM personnel made several measurements of radiometric temperature with a Barnes PRT-5 radiometer.

Information on cultural and vegetative features (cover type, condition, etc.) was obtained for all four sites and additional areas between 9 and 14 September 1973 by ERIM personnel. While not all of this information was used directly in the Skylab processing, it contributed to the general knowledge of the area, and much of it was also of value in the ERTS Ontario study [3] which was ongoing at this time.

Comprehensive meteorologic data for the week preceding the Skylab pass and aircraft flights were obtained from the University of Guelph meterologic station located on the Experimental Research Farm near Elora. Meterologic data was also obtained from the two stations in the Oakville basin and from the Waterloo-Wellington "A" station.

3.2 DATA PROCESSING

3.2.1 DATA SELECTION

One daytime flightline over the Guelph area where specific moisture measurements had been taken was chosen to process and test the ability to infer soil moisture using thermal and/or reflectance data. This data was obtained between 1317 and 1320 (local time) at 5,000 ft above the terrain. Flight direction was SE (135° ground track). Coverage included a portion of Highway 6 between Guelph and Elora, Ontario, Canada and the University of Guelph Experimental Research Farm near Elora. Four of the twelve multispectral bands obtained on this date were selected for processing. It was felt they would be the most useful for accomplishing the study objectives. They are listed in Table 3.

A pre-dawn flight over the Elora Research Farm the following morning (11 September) collected data only in the thermal band. The data was collected between 0645 and 0647 at 1,000 ft.

TABLE 3

BANDWIDTHS SELECTED FOR PROCESSING. Data Obtained by ERIM C-47 on 10 September 1973 using the M7 Scanner

Processed Tape Channel	10% Response Points	50% Response Points
1	0.62 - 0.70 μm	0.63 - 0.67 μm
2	0.67 - 0.94 μm	0.70 - 0.90 μm
3	1.0 - 1.4 μm	1.07 - 1.28 μm
4	9.3 - 11.7 μm	9.53 - 11.54 μm

3.2.2 DATA QUALITY

The quality of the data processed was generally good. Some saturation of the signal occured in the .62 - .70 μm (red) band during data collection, however.

3.2.3 DATA PREPARATION, PREPROCESSING, AND PROCESSING

There are potentially many problems in any data set which, if not corrected, can reduce the accuracy of results obtained using that data. While some of these potential problems are instrument related, others are associated with the radiation environment and the scene being scanned.

Operations to solve these problems which can be done without specific reference to the video (the pictorial representation of the scene scanned) have been designated as data preparation. Operations which utilize the video and are meant to reduce or eliminate those effects which originate outside the scanner have been designated as preprocessing. The data preparation and the preprocessing done with the day data (5,000 ft) and the pre-dawn data (1,000 ft) were different because of differences in data characteristics (no visible bandwidths in the pre-dawn, for instance) and because the two data sets were to be used for different purposes. The flow charts given in Figures 10a and 10b illustrate the general steps undertaken in the processing of both the day and the pre-dawn data. The following paragraphs provide a general discussion of each step.

3.2.3.1 5,000 ft Daytime Data

After selection of the channels to process, a section of one flightline covering several sample sites on the Elora Farm was designated to process. This section of the data on the original analog data tape was then copied. During the copying procedure deskewing was performed, correcting any misregistration between channels, regardless

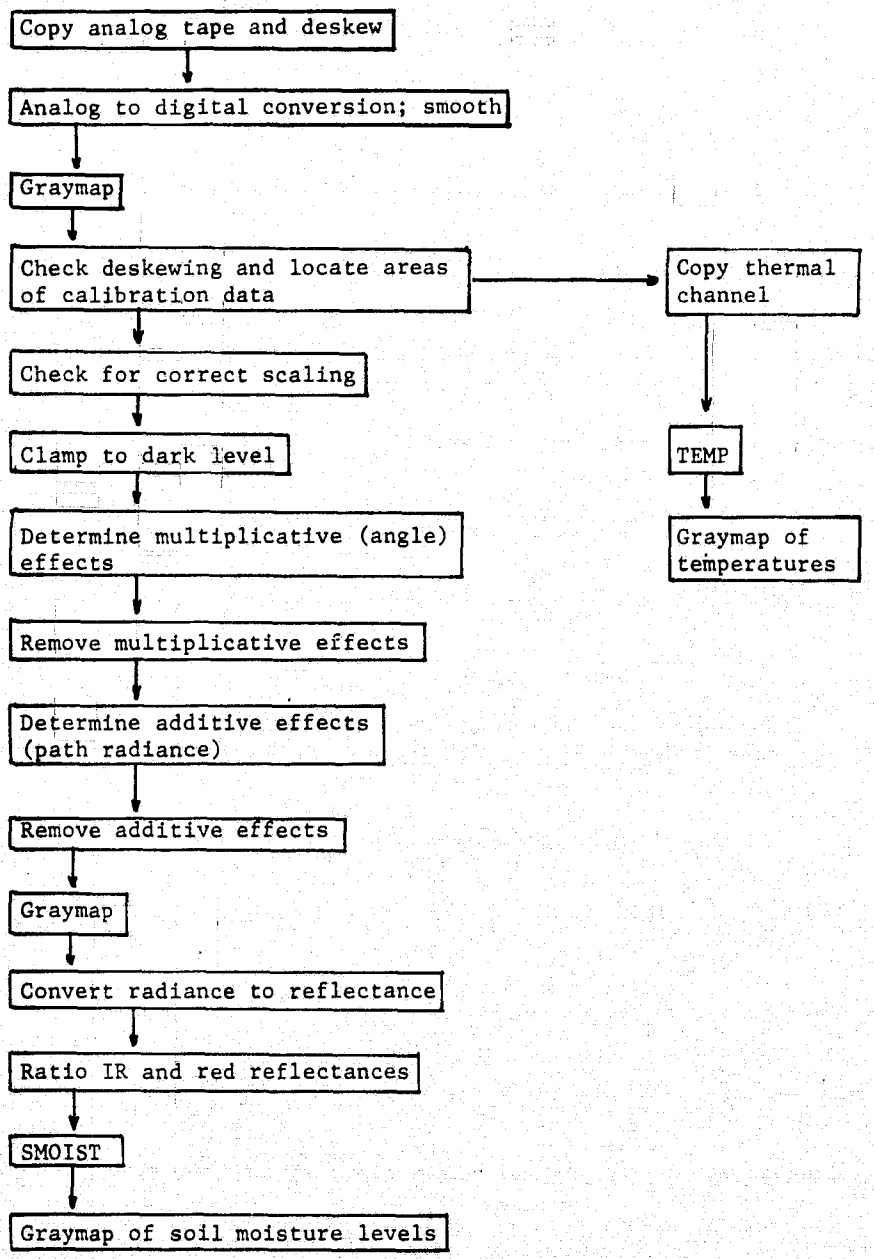

FIGURE 10a. STEPS IN PROCESSING OF THE DAY TIME AIRCRAFT DATA OBTAINED 10 SEPTEMBER 1973 AT 5,000 FEET.

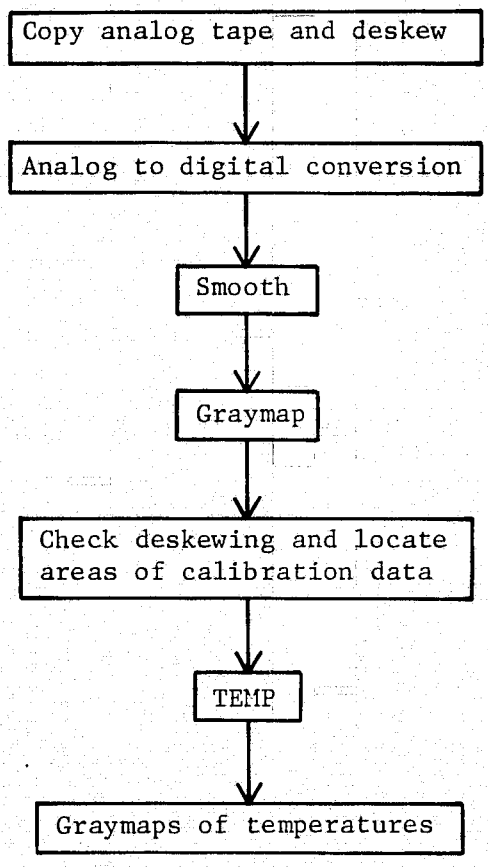

FIGURE 10b. STEPS IN PROCESSING OF THE PRE-DAWN AIRCRAFT DATA OBTAINED 11 SEPTEMBER 1973 AT 1,000 FEET.

of the cause.* Next, the copied analog data was converted to digital format. During this procedure the data was also smoothed by averaging values over several resolution elements. The design of the ERIM M7 scanner is such that at a flight altitude of approximately 1,000 ft and a ground speed of 200 ft per second each revolution of the scanner mirror results in a sample of the terrain which is contiguous with the next scan line area sampled. At higher flight altitudes oversampling results, with the same area being scanned more than once. Using the Zeiss photography and topographic maps, the flight altitude for the portion of the flightline of interest was determined to be 4964 ft. At this altitude and the nominal ground speed, all or part of the same area was sampled every eight scan lines. Rather than correcting the oversampling by dropping scan lines, (in other words, copying only every eighth scan line in this data set), we chose to average every eight lines and use this as the new scan line data. The combining of lines containing largely redundant information also serves to alleviate or reduce problems with system noise. After this step a graymap was produced and the smoothing checked by examining the resulting aspect ratio.

In the next data preparation step the correctness of the deskewing done during the tape copying procedure was confirmed and specific areas of calibration data were located (e.g., hot plate, cold plate, sun sensor). Analysis of the data indicated that no scaling of the data in each band to the sun sensor signal was necessary. In other words, there were no significant gain changes, or variations in scene illumination which would produce the same effect as changing the gain.

---

*The reference signal used for alignment is one which is recorded in each band during data collection as the scan mirror views a reference source in the scanner.

The next data preparation step involved eliminating level shifts by clamping the data for each scan line in each band to the dark level signal. The dark level signal is that signal which is generated when scanning the dark interior of the scanner housing and which theoretically produces zero radiance input to the system.

Preprocessing to eliminate or reduce effects on the data which originate outside the scanner was begun next. The two basic effects which preprocessing techniques strive to remove are additive or multiplicative in nature. The multiplicative or angle effects arise from nonuniform angular responsivity of the scanner,* atmospheric transmittance, and bidirectional reflectance, and are all a function of the scan angle. The radiation incident on an object being viewed at a given angle is multiplied by its reflectance, the transmittance of the atmosphere between the object and the sensor, and the scanner responsivity at that particular angle of view to form the radiation incident on the detector. Additive effects, on the other hand, are the result of path radiance (radiation scattered into the receiver by the atmosphere). Because of the relatively clear atmospheric conditions during data collection, we felt that angle (multiplicative) effects would be more serious than path radiance (additive) effects in our data.

In order to determine the extent of the multiplicative effects in our data and make the calculations necessary to remove them, we first made the assumption that the scene, over its entirety, contained an approximately equal distribution of all objects of interest at all angles. (This has been found to be a valid assumption for farming areas.) The scene was then divided into 70 divisions or "angles" per scan line of 5 data points each. The average signal value of all scan lines within each division was calculated and a parabola fitted to these

*While removal of the effect of nonuniform angular responsivity of the scanner actually falls into data preparation and can be done as a separate step if this nonuniformity is known and fixed, removal of the effect may be accomplished simultaneously with the removal of the other angular effects.

means by least squares. The multiplicative coefficients used to compute the angle corrected data were based on this parabola and were noramalized to the division containing the nadir. An additional program applied these coefficients to the clamped, deskewed, and smoothed data to produce the angle corrected data.

The final preprocessing steps were intended to remove the additive effects due to path radiance. If the reflected radiance at any point is close to zero, either because the reflectance is near zero or the object is in deep shadow, the signal received at the sensor is essentially all path radiance. Using the assumption that the scene contained sources of low reflected radiance, we scanned the entire data set for the ten lowest signal values in each channel. After evaluation of the data, a value was chosen for each channel which was thought to represent the path radiance component of the signal. In all cases, this was the low point on the continuum of low signal values. Finally, this "dark level" value for each channel was subtracted from the entire data set of that channel.

Since use of the reflectance algorithm for determination of soil moisture required reflectance data as input, the next step in the processing was conversion of the data from signal values proportional to radiance to reflectances. There was no completely satisfactory calibration procedure that could be implemented on this data set, but the following procedure was followed.

Targets for which we felt we could estimate the spectral reflectance were identified on a graymap, and conversion factors relating scanner data values to estimated reflectance were determined for channels 1 and 2. Using this information as the initial basis for reflectance calibration, the scanner data was transformed to "reflectance" data. IR/red reflectance ratios of the scanner data for bare soil, which has a known, fairly constant value, were then computed to see if they were reasonable. The final test of the validity of the calibration was

to see if one or two of the values of soil moisture predicted by the soil moisture algorithm were in the same "ballpark" as one or two field measurements of soil moisture.

This final step was only used to test the rather tenuous calibration of the scanner data. The specific algorithm which had been developed was not altered in any way. This procedure causes the average computed values of soil moisture to be somewhere in the right range, but does not affect the relative ordering of the values.

Once suitable calibration factors were determined, they were applied to channel 1 and channel 2 to correct scanner data values to reflectance. Each value in channel 2 (IR) was subsequently divided by the corresponding value in channel 1 (red). Final output was a tape with 3 channels: red reflectances, IR reflectances, and IR/red reflectance ratios, all scaled by a multiplicative factor of ten.

A computer program, SMOIST. (listed in Appendix), was written to implement the soil moisture algorithm developed for use with reflectance data. This algorithm is discussed in Section 6.

SMOIST. initially removes any scaling factor remaining from the conversion to reflectance and ratioing procedures and then squares the IR and the IR/red channels. (A scaling factor is used since only integer output can be written on the output tape and failure to use such a factor results in loss of considerable significance.) The calculations indicated by the algorithm are then performed on each data point in the region designated to be processed. The output listing includes, for each data point within the processed region, the IR reflectance value and the IR/red reflectance ratio (both without scaling factors), the calculated percent soil moisture, and an integer value from 1 to 511. This latter number, optionally written on an output tape, is the scaled result of the soil moisture algorithm calculation. Each integer value is related to a percent soil moisture, from 0 to 100; the relationship is given in a table listed with the output. It is then possible to map levels of percent soil moisture from the output tape.

Several areas of varying percent vegetation cover for which we had point measurements of soil moisture were processed by SMOIST. Results and discussion are presented in Section 6.

3.2.3.2 1,000 ft Pre-dawn Data

Both because of the lower flight altitude at which the pre-dawn data were collected and the fact that only one wavelength region (thermal infrared) was obtained due to the low light level, the data preparation, preprocessing, and processing steps followed for this data set were different than those done for the 5,000 ft (daytime) data.

As with the 5,000 ft data, a copy was made of the section of interest from the original analog data, at which time deskewing was done. Then the data was converted to digital format. Actual flight altitude during collection of the area of interest was determined, as before, and found to be 1042 ft. Some overlap of scan lines was calculated to have occurred at that altitude and the nominal ground speed. Smoothing or averaging of every two scan lines was therefore done. Again, the reasonableness of the smooth was verified using a graymap. The final data preparation step was checking the deskewing and locating areas of specific calibration data, just as was done with the 5,000 ft data.

At this point processing was begun. A copy of the thermal channel from the 5,000 ft data had been made when that data had reached a similar stage in data preparation, so the two were treated together as one data set from this point. A temperature conversion program was used to convert the voltages to radiative temperatures on the ground. The program utilized a linear interpolation between two internally generated sources of known temperature, the hot plate and the cold plate. Temperatures were calculated and mapped for several areas of sampled soil moisture, both day and pre-dawn. Results are presented and discussed in Sections 5 and 6.

4
REMOTE DETERMINATION OF SOIL MOISTURE

In the following sections, results of an investigation of the feasibility of remotely determining surface soil moisture are presented. Two approaches are discussed, one of which uses thermal data and another which uses shortwave reflected data (visible & near IR).

Both approaches are initially analyzed on the basis of theoretical models. Aircraft scanner data is subsequently processed to test the results of modeling. It was anticipated that Skylab S192 data of the same area would be processed in order to extrapolate the results of the aircraft processing. No S192 data over the area of coincident ground and aircraft data were available, so the aircraft results must stand as a low altitude analog of what might be done over very large areas using space data with similar spectral bands.

There are many potential uses for information on surface soil moisture. For example, surface soil moisture is important to hydrologists insofar as it affects the distribution of rainfall into runoff and additions to the soil profile.

Surface soil moisture is important to the agriculturist in its effects on seed germination and early crop development. Soil moisture is of importance to both agriculturist and range manager for inferring potential production of the vegetation resource.

In many of the potential uses of soil moisture information, soil moisture maps that might be produced by remote sensing would be more useful than point samples, or inferences of soil moisture from rainfall data at non-optimally placed meteorological stations.

There are very few land areas that are bare soil for any significant period of time. Bare soil areas tend to be planted by man or become covered by natural vegetation in the somewhat slower process of vegetation succession. Accordingly, the major emphasis in this

effort was to develop a technique for estimating soil moisture under variably vegetated terrain.

The use of thermal data can presently be justified on rigorous theroretical grounds only for bare soil areas, whereas the use of reflectance data can be justified for both bare and partially vegetated areas under certain circumstances. Nevertheless, the usefulness of thermal data in partially vegetated areas was investigated empirically because of our feeling that thermal data may be useful in partially vegetated terrain if we can learn how to interpret it.

5

THERMAL DETERMINATION OF MOISTURE CONTENT OF BARE SOIL

5.1 THERMAL MODEL

A model of the thermal behavior of planar objects under various environmental conditions was developed prior to this project [4] and it has previously been used to study the effects of variations in moisture status of soils [5]. The model was used in this investigation to study the feasibility of using thermal data, especially that collected at two points in time, in an effort to infer surface soil moisture of bare soil areas. Previous investigations [4,5,6,7] had indicated that this might be possible.

The idea that thermal data might be able to give information about the water status of soils is a logical consequence of the thermal properties of soils. For example, the specific heat and thermal capacity of soils is known to increase with an increase in soil moisture [8]. In order to learn more about these relationships, and perhaps even quantify them, we resorted to use of the thermal model. The model is assumed to be useful for bare soil, but not for vegetated soil surfaces.

5.1.1 INPUT PARAMETERS

The environmental factors used as inputs to the thermal model include hourly values of air temperature, wind speed, solar radiation, and cloud cover. A 10-day history of these parameters was used in our calculations. An initial value of soil temperature was also a necessary input. All of these environmental data were furnished by the meteorological station at the University of Guelph Environmental Research Farm at Elora, Ontario.

The soil is divided into 6 layers which are assumed to be homogeneous. In our calculations the layers were: 1) 0-5 cm; 2) 5-15 cm; 3) 15-30 cm; 4) 30-45 cm; 5) 45-60 cm; 6) 60-100 cm.

A surface roughness was specified. In addition, each of the layers was characterized by the following parameters: 1) texture (% sand, silt, and clay); 2) organic content; 3) bulk density; 4) conductivity; 5) diffusivity; and 6) moisture content.

The values for most of these parameters were derived largely from theoretical values for Guelph loam described by De Vries in Van Wijk [9]. Many of the sites of interest in the study area were occupied by Guelph loam and similar soils.

5.1.2 RESULTS OBTAINED FROM MODELING

Four surface (0-5 cm) soil moisture conditions (and resulting profiles to 100 cm) spanning the range of soil moisture variability found on the experimental site were simulated by modeling. The albedo of the soil surface was not assumed to change as soil moisture changed. The resulting surface temperature as a function of time over the period when scanner data was collected is shown in Figure 11.

One of the more conspicuous features of this graph is the cross-over of the temperature curves going from day to night. The driest soil is warmest during the day and coldest at night. This gives theoretical support to the hypothesis that the difference in temperature (day-night) should be a good indicator of the relative moisture content of a particular kind of soil.

Temperature differences (day-night) for the four soil moisture states indicated in Figure 11 are plotted against soil moisture in Figure 12. As can be seen, there is a nearly linear relationship between temperature difference and soil moisture over this range of

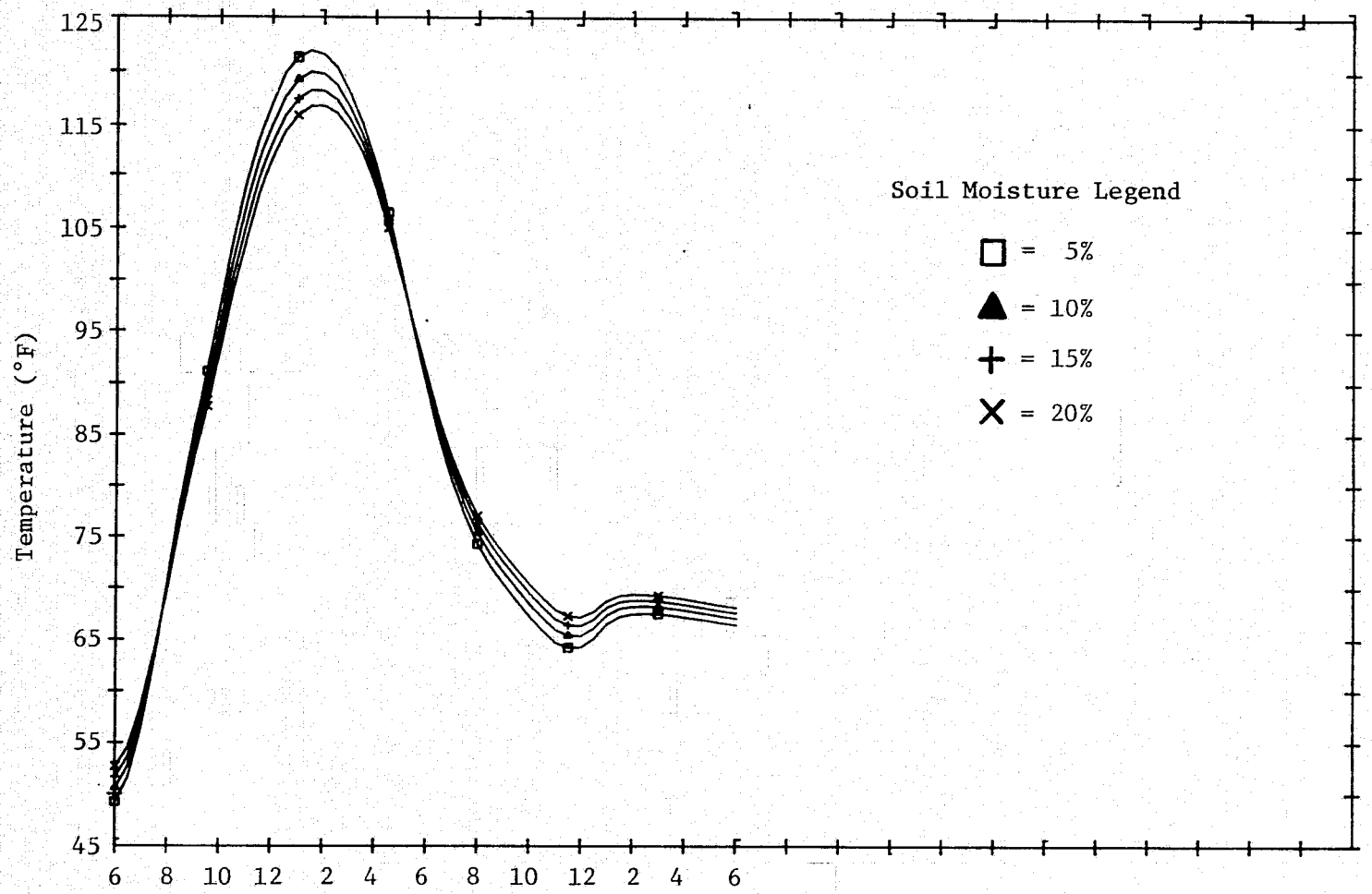

FIGURE 11. CALCULATED SURFACE TEMPERATURE VS TIME FOR FOUR VALUES OF SOIL MOISTURE.

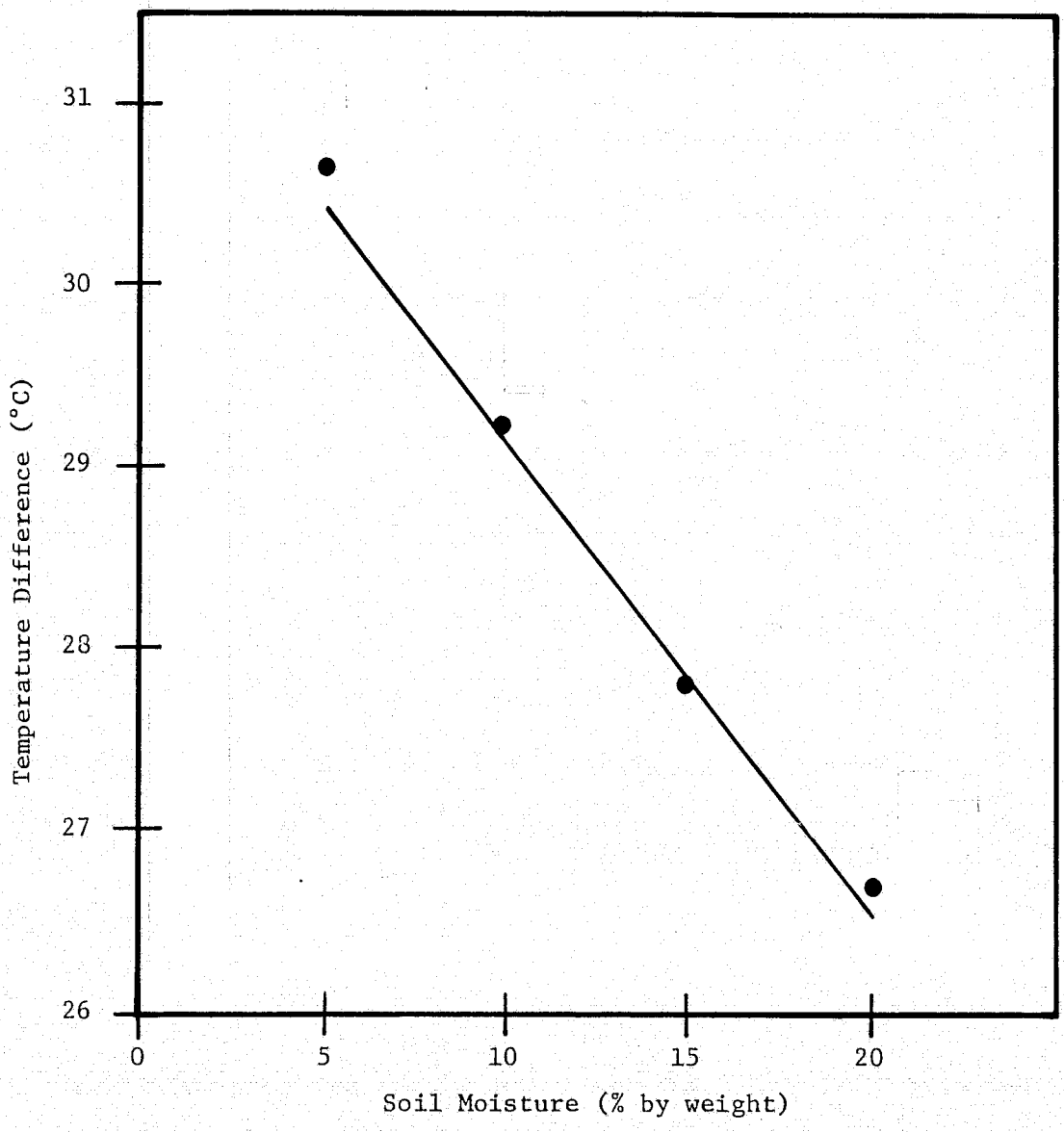

FIGURE 12. MODELED TEMPERATURE DIFFERENCE (day-night) VS. SURFACE SOIL MOISTURE FOR GUELPH LOAM.

values of soil moisture. Such information is one of the potentially useful results of modeling such as this.

5.2 RESULTS OBTAINED FROM SCANNER THERMAL DATA

Only three bare soil areas for which field soil moisture data was available were also present on the aircraft scanner data which was processed. Only two of these three fields had scanner data available for both day and night (pre-dawn). However, ground-collected thermal radiometric measurements were made in the pre-dawn hours using a PRT-5. These measurements indicated very little temperature variation ($< 0.5°$) between bare soil fields with different soil moistures at the pre-dawn period of time. Accordingly, it was decided to use just the day-time thermal scanner data for investigation of the relationship to soil moisture so that at least three points could be examined. The modeling which was previously done indicated that mid-day temperature, by itself, would be highly correlated with soil moisture (Figure 11).

The pre-dawn scanner data indicated that the two bare soil fields imaged had radiometric temperatures of slightly over 16°C. The field radiometric measurements of the same two fields were approximately 15°C, thus indicating that the thermal scanner data was approximately correct, at least at one temperature. No day-time field radiometric measurements were made in this area.

Only one field measurement of soil moisture was made at each site at a given time (i.e., day and/or night). Unfortunately, a single measurement of soil moisture has been found to be rather unreliable [10]. Field values of soil moisture obtained for the same site during the day and pre-dawn showed no consistent relationship to each other (i.e., one was not always higher or lower than the other). Therefore, it was decided to average the two readings to obtain the "best" estimate of soil moisture. This averaging was only possible

on two of the three bare soil areas, however, since one of the day measurements of soil moisture was not made.

Scanner-recorded temperatures for the six pixels closest to the point at which the field measurements were made were averaged and compared with the field measurements of soil moisture. The results are presented in Table 4.

There is a lack of a consistent relationship between temperature and soil moisture for these three sites. However, with so few points, it is not possible to draw any definitive conclusions regarding these results. It is possible that if we had been able to use both day and night scanner temperatures, and if we had more sample sites and better estimates of soil moisture, our results might have been improved.

5.3 COMPARISON OF MODELED RESULTS WITH SCANNER RESULTS

The thermal model did not predict actual temperatures of soils at different moisture contents at different points in time. For example, the modeled (predicted) temperatures of site 34 (4.6% soil moisture) were 19.2°C pre-dawn and 49.8°C day, a difference of 30.6C°. The scanner-recorded radiant temperatures for the same site were 16°C and 35.5°C, a difference of 19.5C°.

For a true comparison of these numbers, the modeled "actual" temperatures should be multiplied by some realistic value of emissivity (such as 0.9), and some correction of the scanner data for the effects of atmospheric water vapor should be made. It seems unlikely, however, that these corrections would result in a good quantitative agreement between the scanner data and the modeled data.

This fact is not necessarily a reflection on the accuracy or validity of the model, however, since many of the important input parameters to the model had to be estimated. But since such estimations

TABLE 4

SCANNER TEMPERATURE AND FIELD DETERMINED SOIL MOISTURE

SITE	SCANNER TEMPERATURE	SOIL MOISTURE (% BY WEIGHT)
13	34.97	13.98
14	34.12	8.18
34	35.16	4.06

will almost always have to be made, the thermal model should probably not be used to try to predict exact soil temperatures as a function of soil moisture. Rather, the model will be useful for such things as investigating the consistency of any relationship between temperature and soil moisture for a variety of soil types and weather histories.

The model could also be useful for predicting the NEΔT required by satellite systems such as the S192 for determining soil moisture. Present indications are that the NEΔT would have to be smaller than that which is available in the S192 package.

6

DETERMINATION OF SOIL MOISTURE IN VARIABLY VEGETATED TERRAIN

The ability to assess soil moisture of bare soil areas would certainly be useful. However, the ability to assess soil moisture in variably vegetated terrain would be even more valuable. It was with this thought in mind that consideration was given to developing such a capability. Because of the difficulty in interpreting thermal information in vegetated terrain, it was decided to emphasize utilization of reflective (visible and near IR) information for determination of soil moisture in vegetated terrain.

6.1 THE REFLECTANCE SOIL MOISTURE MODEL

6.1.1 BASIC CONSIDERATIONS

Before describing the development of the soil moisture model for variably vegetated terrain, some of the important basic relationships involved in such a model will be reviewed. Reflectance bare soil has been found to decrease with increasing soil moisture, at least over most values of soil moisture (Figure 13). The difference in reflectance between wet and dry soils has been found to be greater in the reflective IR spectral region than in the visible part of the spectrum. Therefore, it would be desirable to use an IR spectral band as the primary source of information on surface soil moisture.

Reflectance of vegetation canopies as a function of the amount of vegetation present has been found to be very spectrally dependent [11] (Figure 14). Generally, as the amount of green vegetation cover increases, the near IR (0.7 - 1.1 μm) reflectance increases. However, red reflectance generally decreases with vegetation cover.

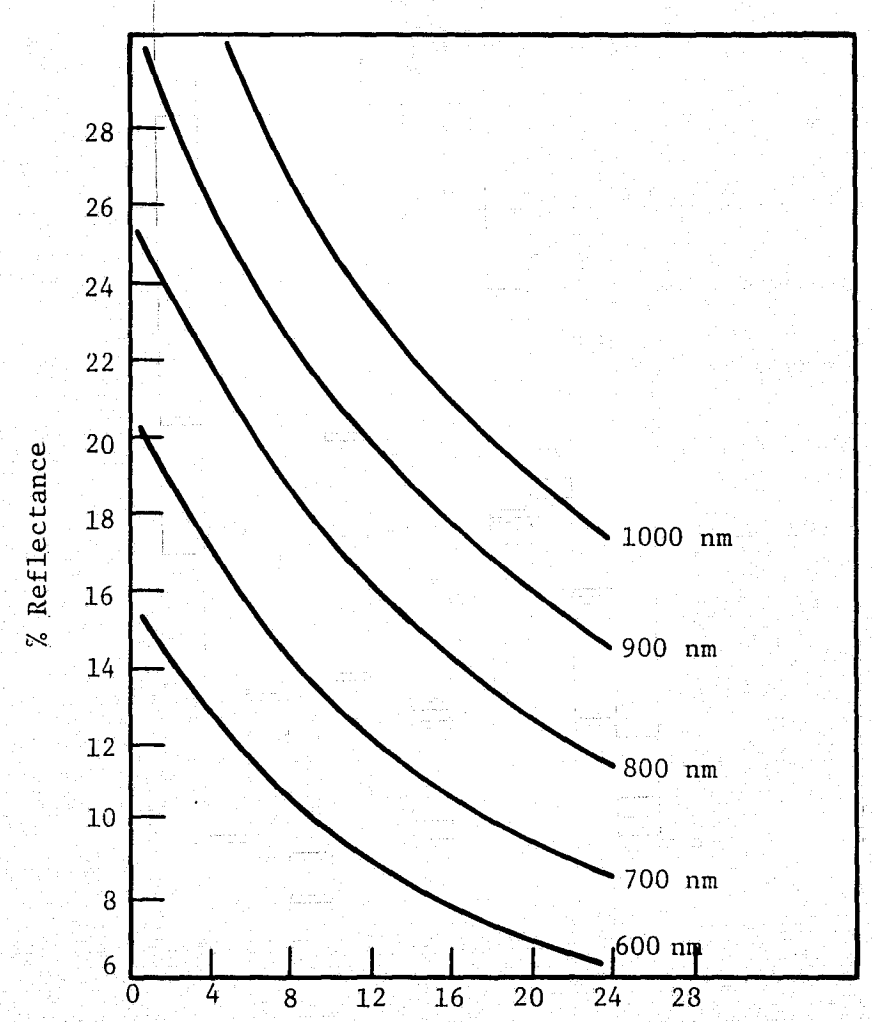

FIGURE 13. PERCENT REFLECTANCE VS PERCENT SOIL MOISTURE AT VARIOUS WAVELENGTHS [After Bowers and Hanks, 1965].

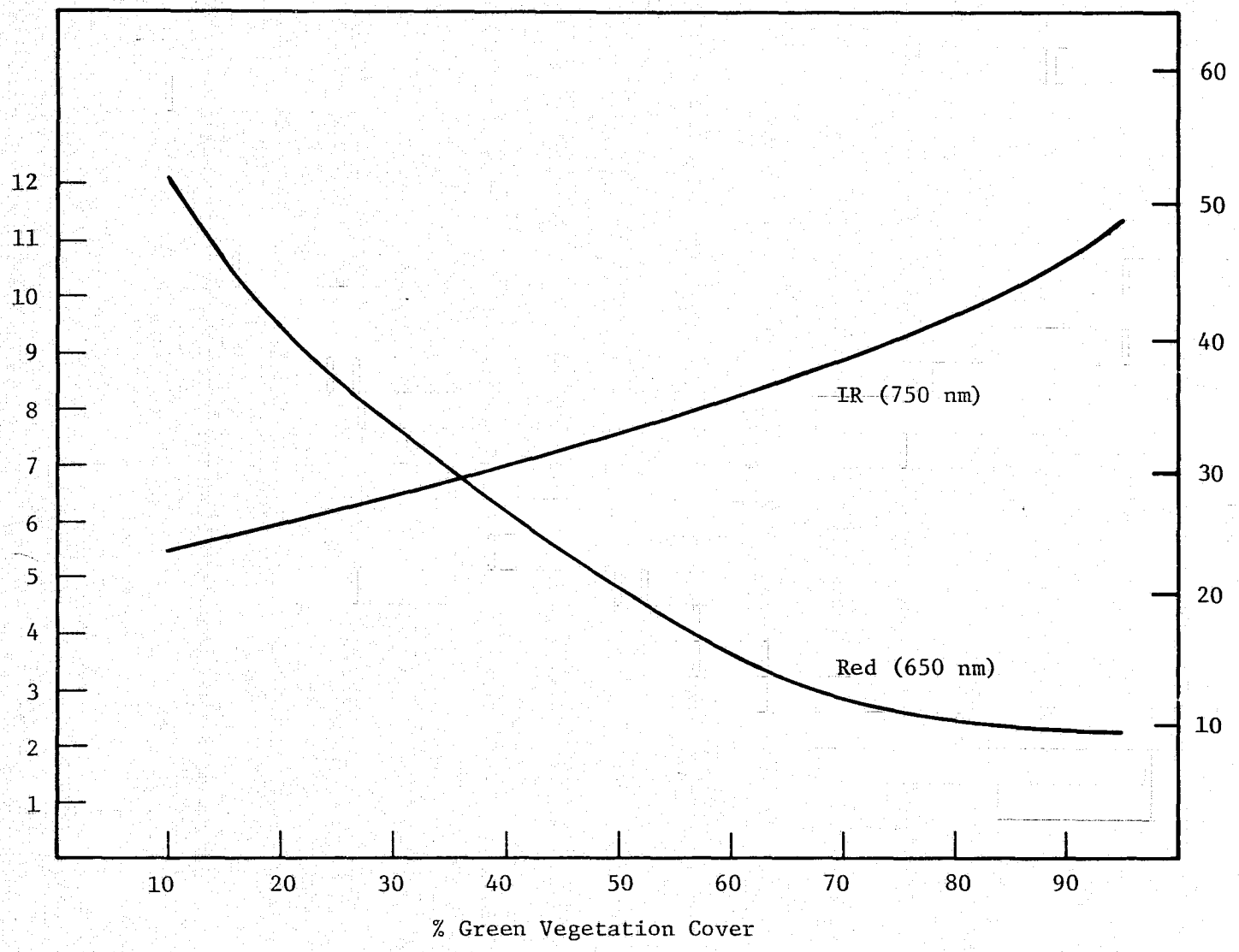

FIGURE 14. EFFECT OF VEGETATION COVER ON RED (650 nm) AND NEAR IR (750 nm) REFLECTANCE.

In order to infer soil moisture of terrain which is covered with a variable amount of vegetation cover, some means has to be devised to account for the effects of vegetation cover. The problem is to devise a way to account for the amount of vegetation cover independent of the effects of variable soil moisture.

Fortunately, there appears to be a solution to this problem. Since the effects of vegetation cover have opposite effects on the IR reflectance and the red reflectance, and IR/red reflectance ratio is more sensitive to the amount of vegetation cover than either spectral band individually. On the other hand, an IR/red reflectance ratio is rather insensitive to soil moisture, as is shown in the ensuing discussion.

We analyzed data from Bowers and Hanks [12] for a loamy sand and found reflectance ratio data to be quite insensitive to soil moisture (Table 5). For five measurements between 1% and 13.3% soil moisture, the standard deviation of the ratio of reflectance at 750 nm to 650 nm was less than 3% of the mean value. Similar, although not quite as constant values were found for 850/650 ratios and 950/650 ratios. The insensitivity of an IR/red reflectance ratio to soil moisture appears to be due to the fact that increasing soil moisture decreases the reflectance in the red and near IR regions different absolute amounts, but approximately the same proportionate amount.

Additional evidence comes from data collected by Condit [13]. Condit measured the hemispherical spectral reflectance of a large variety of soils and soil materials (sand, silt, and clay) found in the United States. We calculated the means and standard deviations of the reflectance values in individual spectral bands for 30 of these samples in both the wet and dry condition and found the standard deviation to be as great as 64% of the mean value. We subsequently calculated reflectance ratios for the wet and dry states and found the corresponding values to be quite similar to each other, especially for

TABLE 5

REFLECTANCE RATIOS OF DERBY LOAMY SAND
AS A FUNCTION OF SOIL MOISTURE
(AFTER BOWERS AND HANKS, 1965)

	RATIO		
SOIL MOISTURE	750/650	850/650	950/650
1%	1.38	1.67	2.00
2.6%	1.39	1.71	2.13
5.7%	1.48	1.76	2.25
8.05%	1.42	1.85	2.27
13.3%	1.44	1.88	2.22
mean, $\bar{x}$	1.42	1.77	2.17
standard deviation, σ	.04	.09	.11
$\sigma/\bar{x}$	.028	.051	.051

the 750/650 reflectance ratio (Table 6). When the dry and wet 750/650 reflectance ratios were pooled the mean value was 1.19 and the standard deviation (.11) was only 9% of the mean value. Therefore, the 750/650 reflectance ratio (and to a lesser extent the other two ratios) appears to be useful in normalizing the effects of both soil type and soil moisture.

The most significant aspects of the foregoing material for development of a soil moisture model are summarized in Figure 15. IR reflectance of bare soil decreases with soil moisture. IR reflectance of vegetation canopies increases as the amount of vegetation (% vegetation cover) increases. An IR/red reflectance ratio of bare soil is rather constant with soil moisture, but it increases substantially as the amount of vegetation increases. These concepts are the building blocks from which the soil moisture algorithm was developed.

6.1.2 DEVELOPMENT OF THE REFLECTANCE SOIL MOISTURE MODEL

The basic relationship in developing the soil moisture model is that the soil moisture of bare soil is some function of IR reflectance that may be approximated by the equation:

$$\text{Soil Moisture} = A - B\rho(IR) - C\rho^2(IR).$$

The negative coefficient of B is due to the negative correlation between IR reflectance and soil moisture. The squared term is included as a partial correction for the curvilinear nature of the relationship between soil moisture and IR reflectance (see Figure 13).

As vegetation is added to the scene, we need to make a correction to the bare soil algorithm that will account for the effects of the vegetation. This procedure cannot improve on the basic algorithm; it can only maintain its validity under conditions of variable vegetation cover.

TABLE 6

REFLECTANCE RATIO VALUES FOR
30 SAMPLES IN WET AND DRY CONDITION
(RAW DATA DERIVED FROM CONDIT, 1970)

	REFLECTANCE RATIO					
	750/650		850/650		950/650	
	DRY	WET	DRY	WET	DRY	WET
mean, $\bar{x}$	1.19	1.20	1.25	1.28	1.36	1.40
standard deviation, σ	.12	.11	.21	.23	.36	.43
$\sigma/\bar{x}$	.10	.09	.17	.18	.26	.31

FIGURE 15. THE RELATIONSHIPS FROM WHICH THE SOIL MOISTURE ALGORITHM WAS DEVELOPED

Since the IR/red reflectance ratio is quite sensitive to the amount of vegetation and quite insensitive to the soil moisture (and soil type), it furnishes the basis for our correction.

The effect of an increasing amount of vegetation is to increase the reflectance of the entire soil/vegetation complex (the vegetation canopy) without any change in soil moisture. With no correction, the basic soil moisture algorithm would predict too low a value of soil moisture. Therefore, we must add to the algorithm a positive correction for vegetation cover. The resulting algorithm has the form:

$$\text{Soil Moisture} = A' - B'\rho(IR) \pm C'\rho^2(IR) + D'\rho(IR)/\rho(Red)$$

$$\pm [\rho(IR)/\rho(Red)]^2$$

where the $\rho^2(IR)$ term is a correction for the nonlinearity of the effects of both soil moisture and vegetation, and the $[\rho(IR)/\rho(Red)]^2$ term is a correction for the non-linearity of the relationship between % cover and the IR/red reflectance ratio.

6.1.3 DEVELOPMENT OF SPECIFIC REFLECTANCE SOIL MOISTURE ALGORITHM

In order to determine the values of the specific coefficients of a soil moisture algorithm we made use of a model of vegetation canopy bidirectional spectral reflectance [14]. This model computes the bidirectional spectral reflectance once the following parameters are specified.

1. density, arrangement, and radiometric properties of the biological components of the vegetation canopy (e.g., leaves and stalks).
2. reflectance of the soil background.

3. viewing geometry, including polar look angle, polar sun angle, and azimuth angle.

A generalized herbaceous vegetation canopy was simulated with varying amounts of biological components (vegetation cover). All of the components were assumed to be live and green. Reflectance of a particular kind of soil at various amounts of soil moisture was inferred from data in the literature [12]. Viewing geometry approximating the conditions of the aircraft data collected in Canada were used.

Using the above information the bidirectional spectral reflectance of a number of canopies with varying amounts of soil moisture and vegetation cover were determined. Virtually no information on soil moisture can be obtained from reflectance data when no illuminated soil can be seen. The IR canopy reflectance of canopies with "wet" and "dry" soil at various values of vegetation cover were compared. It was found that the difference in IR canopy reflectance for the two soil conditions fell from 9.5% at low vegetation cover to 2.2% at 63% vegetation cover. A 2.2% reflectance difference between canopies with wet and dry soil was arbitrarily considered the limiting value, and a specific soil moisture algorithm was subsequently developed for terrain which contained up to 63% green herbaceous vegetation. This was done by simulating the reflectance of canopies with 30 combinations of soil moisture and vegetation cover, and subjecting the resulting data to standard least-squares regression to predict soil moisture using the general form of the algorithm which was developed earlier. The resulting algorithm was

$$\text{Soil Moisture} = 19.79 - .02\rho(\text{IR}) + 5.06\ \rho(\text{IR}/\rho(\text{Red}) - .066\ \rho^2(\text{IR}) - .067\ [\rho(\text{IR})/\rho(\text{Red})]^2$$

The R^2 value for this algorithm was 0.95, indicating that the algorithm is highly effective at correcting for the effects of variable vegetation cover, and for accurately predicting the soil moisture.

Modeling such as this can be useful in determining sensor requirements (spectral bands and signal to noise) for future satellite systems for specific applications. For example, our modeling suggests that an NE$\Delta\rho$ of 0.5% or better might be required in the near IR spectral band for estimating surface soil moisture in variably vegetated terrain.

6.1.4 IMPLEMENTATION OF ALGORITHM USING SCANNER DATA

The next step in our investigation of the ability to determine surface soil moisture under conditions of variable vegetation cover was to apply the soil moisture algorithm to reflectance calibrated aircraft scanner data collected over the Elora Farm area of Ontario, using the SMOIST. program described in Section 3.

When the scanner data had been processed using SMOIST., the output was analyzed to assess its performance. Unfortunately, many of the sites at which field determinations of soil moisture had been made were not sites that fulfilled the assumptions of the model. These included sites that were nearly completely covered with vegetation, and sites that had appreciable dead vegetation, such as stubble. However, it was possible to find seven sites which generally fulfilled the important assumptions of the soil moisture model and for which we had obtained field data on soil moisture. These sites included three that were bare soil and four that had up to 60-70% predominantly green vegetation cover. The three bare soil areas had very similar IR/red reflectance ratios of 1.30, 1.32, and 1.38, thereby fulfilling one of the assumptions of the algorithm.

A comparison of the SMOIST. processed scanner data and field determinations of soil moisture is presented in Figure 16. Due to the

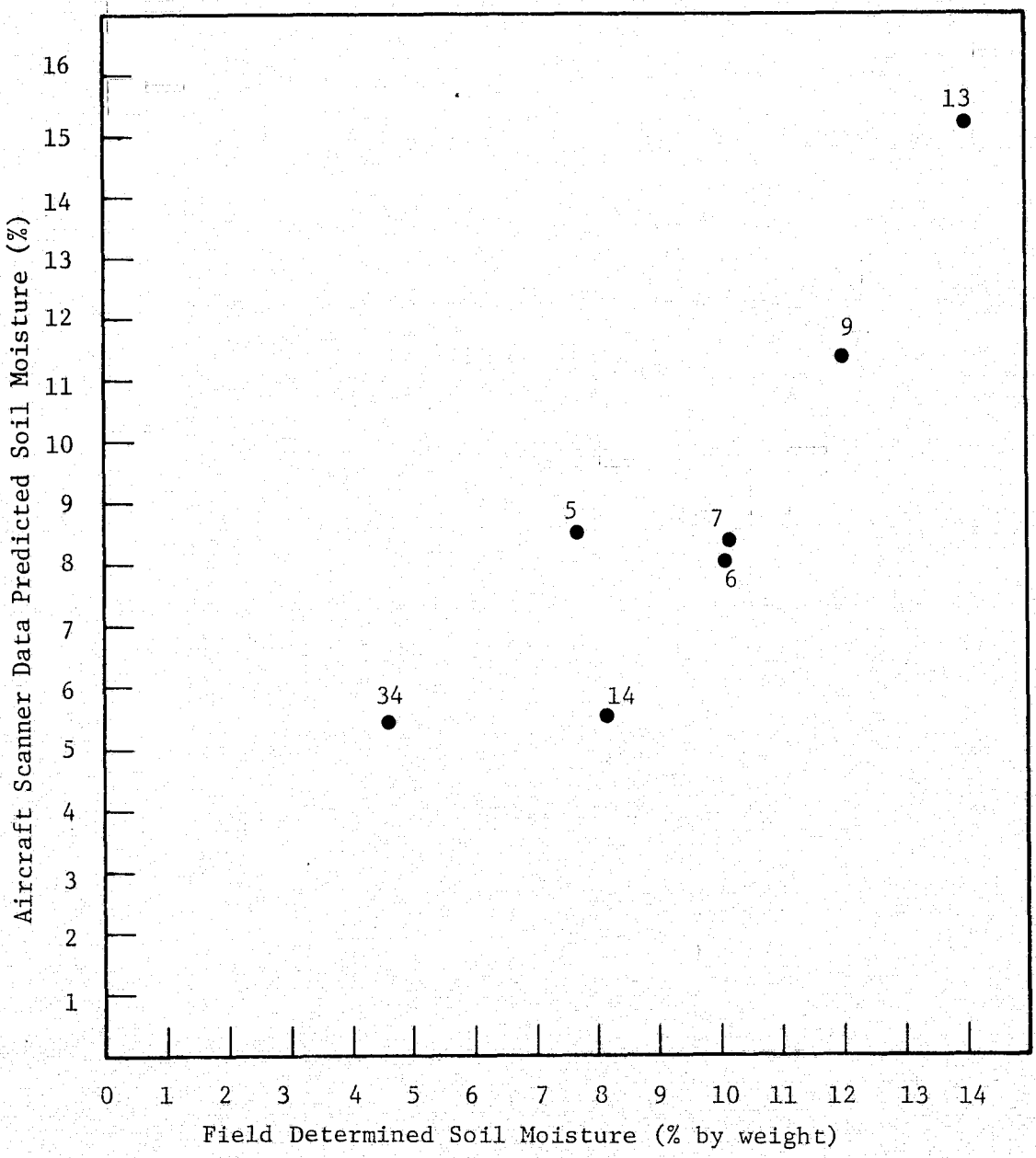

FIGURE 16. SOIL MOISTURE AS PREDICTED USING SMOIST. PROGRAM TO IMPLEMENT SOIL MOISTURE ALGORITHM VS. FIELD MEASUREMENTS OF SOIL MOISTURE.

method of calibrating the scanner data to reflectance (see Section 3), the only meaningful comparison is the ordering of the points. In this respect there is reasonably good agreement between the scanner and field determinations of soil moisture. The target with the greatest soil moisture has the highest value predicted by the scanner data, and the driest soil site has the lowest predicted value. With the exception of site 5, the ordering of predicted soil moisture for the variably vegetated terrain is the same as the field determinations of soil moisture. That site number 5 is in error is not very surprising in that it has the highest scanner-indicated vegetation cover (IR/red reflectance ratio), and is probably near the threshold of IR reflectance insensitivity to fluctuations in soil moisture.

It should be pointed out that the soil moisture algorithm was developed for vertical viewing conditions. The seven fields which were sampled were not all at the nadir, and no correction for the effect of look angle was attempted. This situation will degrade the performance of the algorithm somewhat. However, all of the points were less than 20° off nadir. In addition, it is expected that the IR/red ratio will be somewhat useful in correcting for effects of "projected" vegetation cover at angles off the nadir so that the performance of the soil moisture algorithm should not be severely degraded.

The linear correlation between scanner indicated values of soil moisture and field determinations of soil moisture is 0.89. A linear regression gives an R^2 value of 0.79 with a standard error of 1.5. The relationship is significant at the 99% level of confidence.

Results based on so few points are, of course, not conclusive, but they tend to substantiate the usefulness of the soil moisture algorithm, and demonstrate one possible way in which the algorithm could be implemented. A more accurate way would be to calibrate the coefficients of the soil moisture model to a particular type of situation using a "training" set of data, but we did not have enough points of known soil moisture to try that with this data set.

The advantage of a remote sensing approach to determination of surface soil moisture under variably vegetated terrain is not for making point estimates of soil moisture at a small number of isolated points. Rather, the potential advantage of remote sensing is to infer soil moisture continuously over large areas, thereby facilitating location of homogeneous areas and boundaries between them. In order to demonstrate this potential, a map of soil moisture over a portion of the Elora Farms test site which met most of the assumptions of the model was printed out and is shown in Figure 17. The spatial variation in soil moisture is easily seen.

To test the usefulness of the vegetation correction in the soil moisture algorithm, scanner determined IR reflectance, by itself, was regressed against field determinations of soil moisture. The distribution of the data points is shown in Figure 18. The resulting R^2 value was .06, with a standard error of 3.2. The relationship is not statistically significant.

In addition, a level slice of the IR band was done for the same area as the SMOIST. map of Figure 17 and is shown in Figure 19. The density of the symbols was chosen so that the least dense would indicate highest reflectance (lowest soil moisture in non-vegetated terrain). The substantial differences in the patterns of this map compared with the SMOIST. map reinforce the hypothesis that IR reflectance, alone, can not be used to assess soil moisture in variably vegetated terrain.

6.2 THERMAL INFORMATION IN PARTIALLY VEGETATED TERRAIN

The thermal model is only valid for bare soil, and the relationship between radiometric temperature and soil moisture in vegetated canopies is a complex and incompletely understood phenomenon. Nevertheless, we looked at the scanner radiometric temperatures of several vegetated canopies to see what they would indicate. The results for both bare

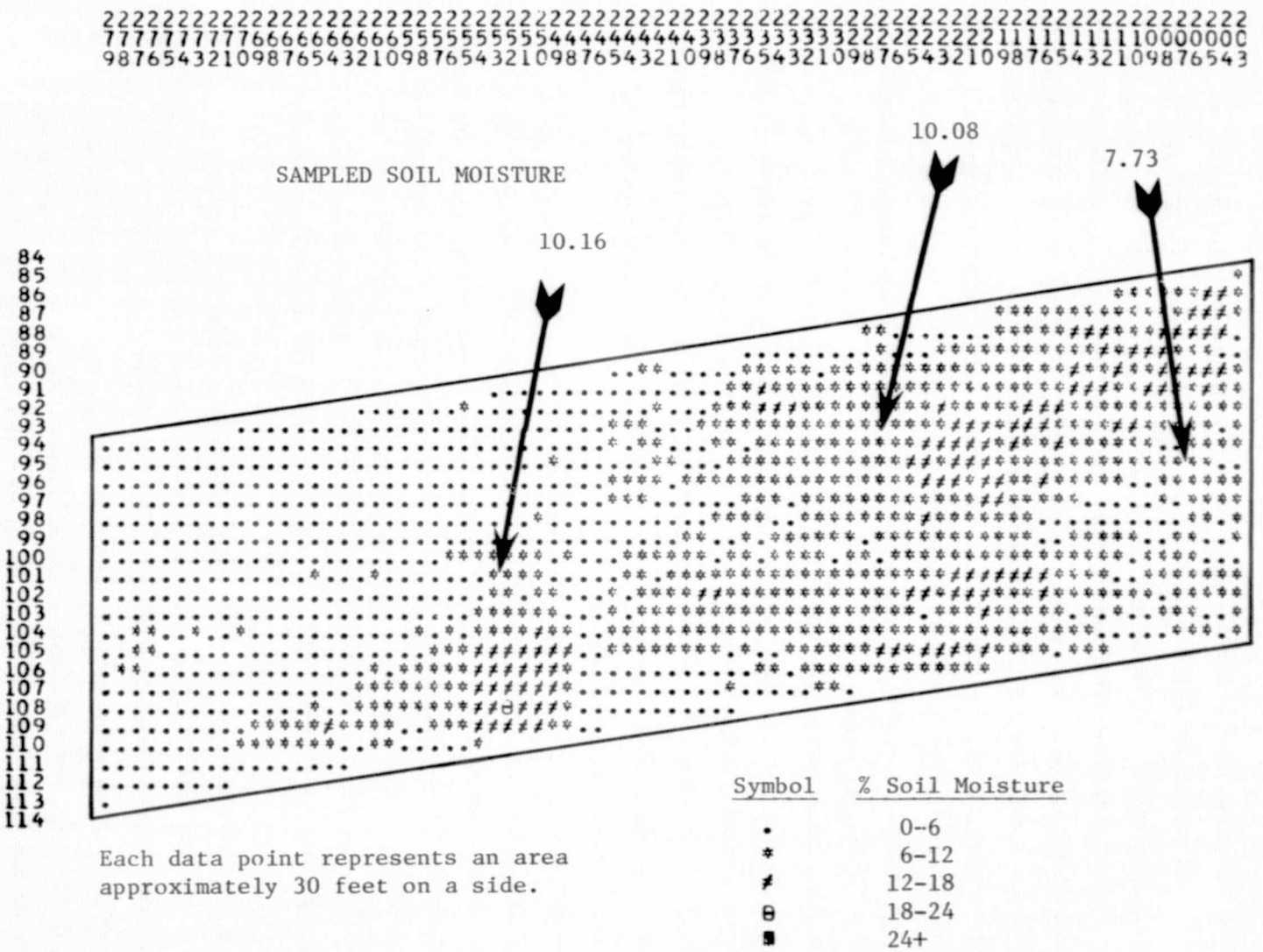

FIGURE 17. A MAP OF SCANNER-INDICATED SOIL MOISTURE (Portion of Elora Research Farm, Ontario, Canada)

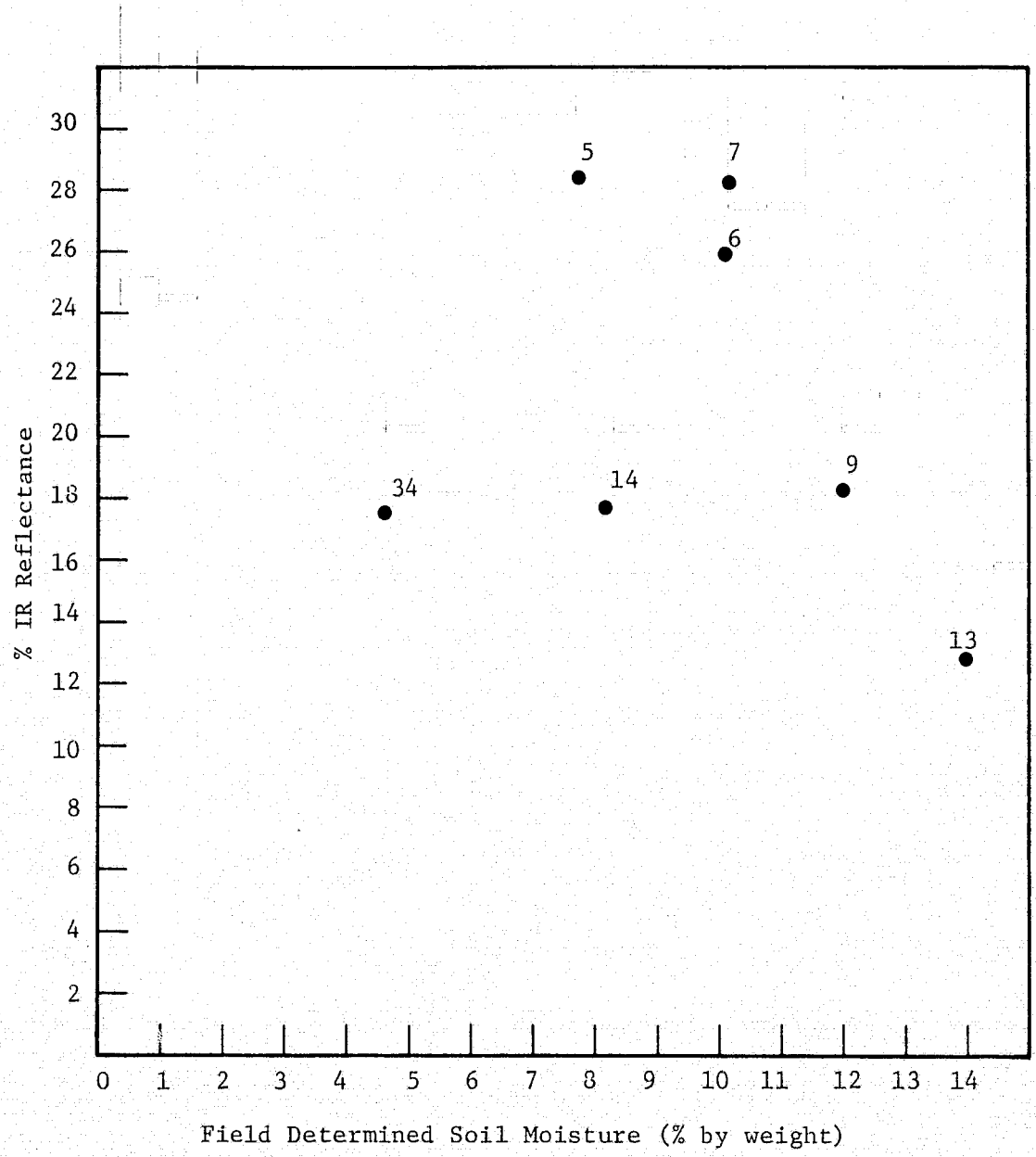

FIGURE 18. SCANNER INDICATED IR REFLECTANCE VS. SOIL MOISTURE.

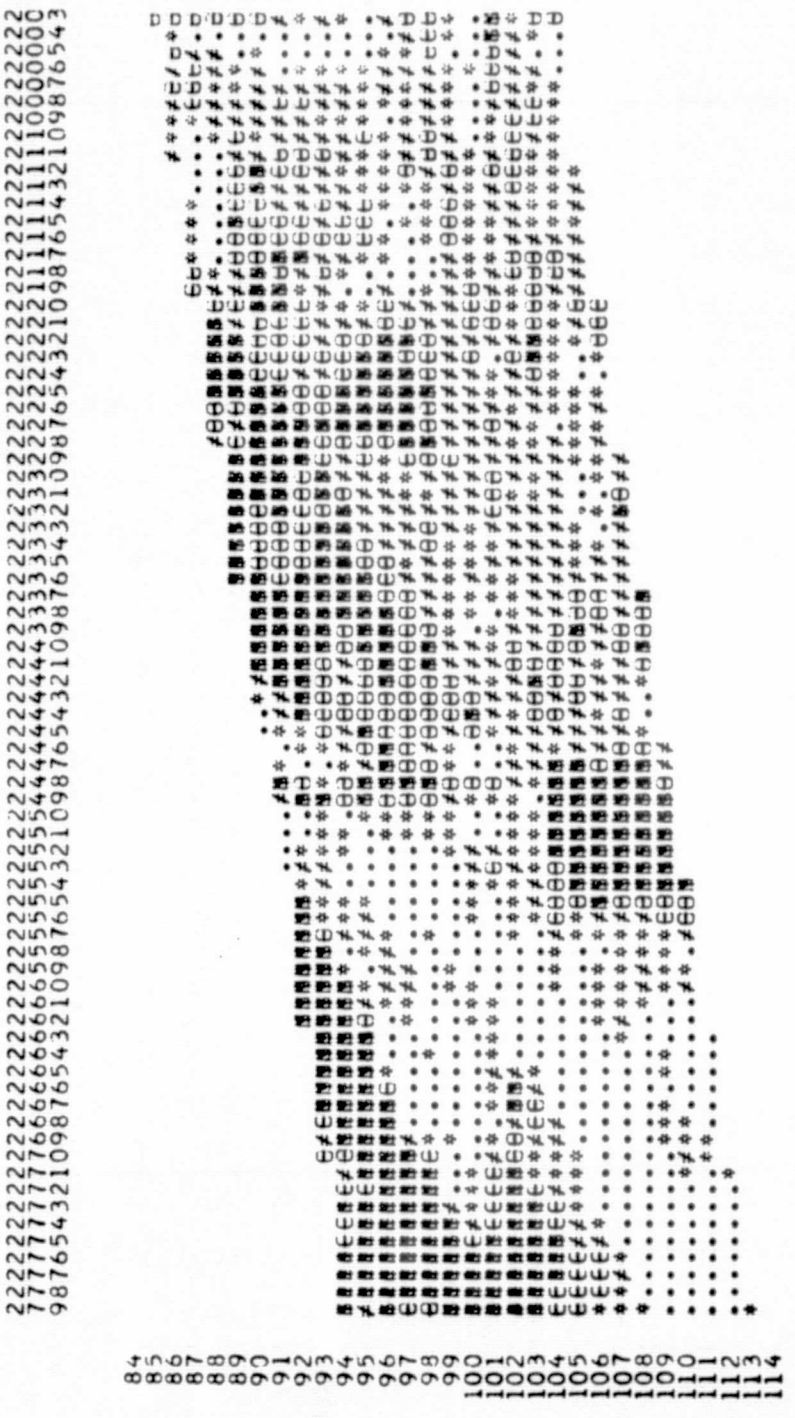

FIGURE 19. AN IR LEVEL SLICE OF SAME AREA AS FIGURE 17 (least dense symbol is highest reflectance).

soil and partially vegetated areas are presented in Figure 20. A regression of scanner temperatures vs. soil moisture gives an R^2 value of .01 and a standard error of 6.4.

A level slice of the thermal band was done for the same area as the SMOIST map of Figure 17, and it is presented in Figure 21. The density of the symbols was chosen so that the most dense symbols indicated highest temperature. The significant differences between the thermal map and the SMOIST map indicate that thermal data can not be used to infer surface soil moisture under variably vegetated canopies.

6.3 ANALYSIS OF SCANNER THERMAL RESULTS IN VEGETATED TERRAIN

On theoretical grounds one would expect the scanner thermal (temperature) data to be most useful in inferring soil moisture for the bare soil fields, sites 34, 14, and 13. However, there is no obvious relationship for these three sites.

On the other hand, there is reasonably good agreement between soil moisture and temperature for the partially vegetated sites. However, the trend is the opposite of what would be predicted on theoretical grounds for bare soil; i.e., the correlation between temperature and soil moisture is strongly positive. The reasons for this correlation are not known, but it should be noted that where IR/red reflectance ratios of these areas were computed from the scanner data, there is also a good correlation found between the thermal data (temperature) and % vegetation cover as inferred from the IR/red reflectance ratios. The warmest target has the least inferred vegetation cover, and the coolest target has the greatest inferred vegetation cover. This can be seen by a comparison of the thermal map and an IR/red level slice map (Figure 22) in which the densest symbols represent the lowest values of IR/red ratios (and inferred vegetation cover). Perhaps,

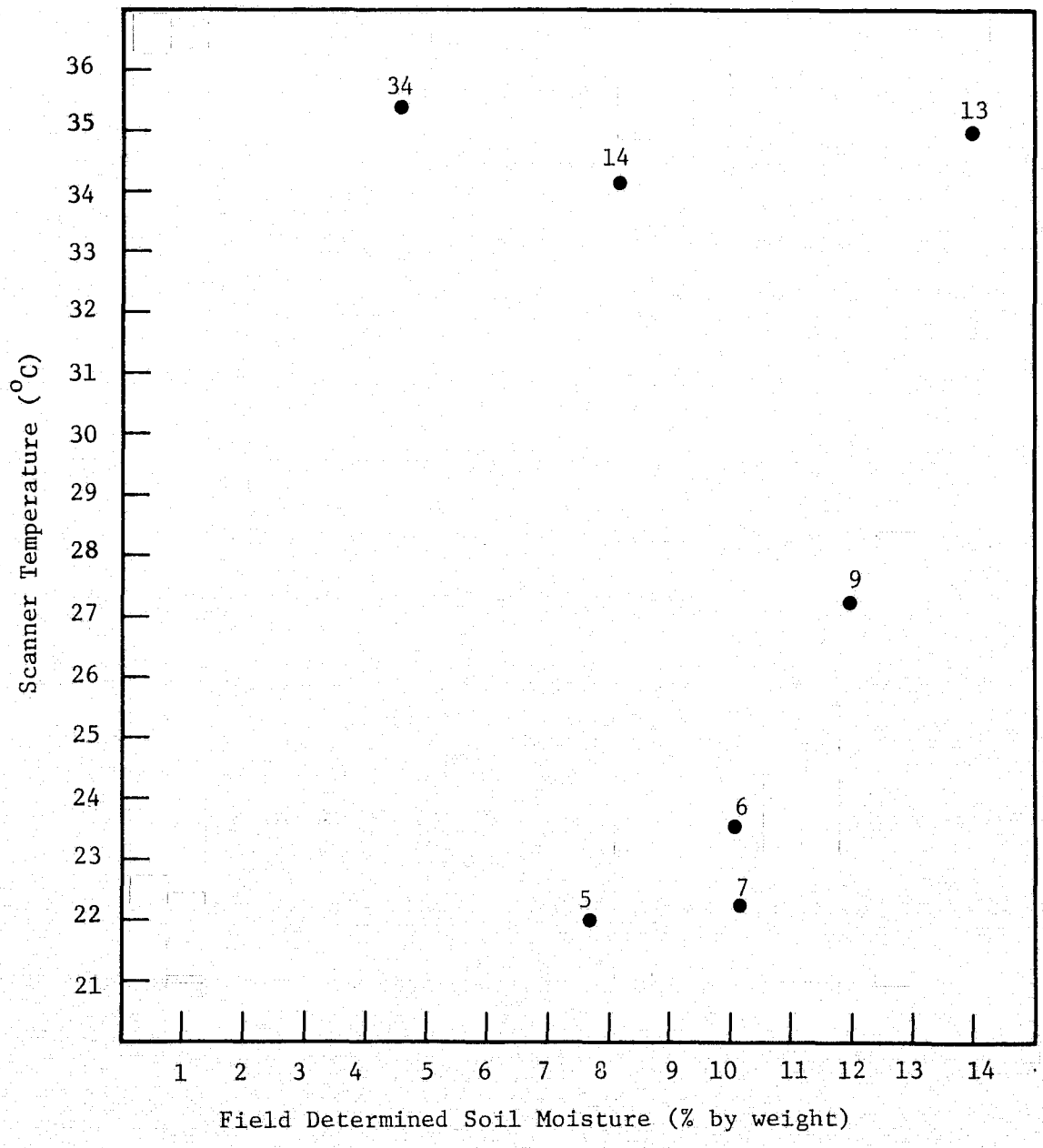

FIGURE 20. SCANNER TEMPERATURE VS. SOIL MOISTURE FOR BARE SOIL AND PARTIALLY VEGETATED TERRAIN.

FIGURE 21. A THERMAL LEVEL SLICE OF SAME AREA AS FIGURE 17 (most dense symbol is highest temperature).

FIGURE 22. AN IR/RED REFLECTANCE LEVEL SLICE OF SAME AREA AS FIGURE 17
(most dense symbol is lowest IR/Red reflectance ratio).

then, we are monitoring differences in temperature that are due to the differential amount of evapotranspiration from the vegetation canopies. The wind speed at the time the data was collected was about 12 mph. enough to cause considerable evaporative cooling. Another possible explanation is that there is more area shaded from the sun's rays (and hence cooler) in the highly vegetated target than in the sparsely vegetated target.

6.4 COMPARISON OF THERMAL AND REFLECTIVE TECHNIQUES FOR DETERMINATION OF SOIL MOISTURE

It is difficult to make conclusions concerning the usefulness of thermal and reflective data for determination of soil moisture based on the limited data presented in this report. Thermal modeling indicated that thermal data would be useful for determination of soil moisture for bare soil areas. The few (3) empirical data points we had to test this hypothesis were inconclusive. One problem seems to be the small changes in temperature with soil moisture. Another problem with using thermal data, as we see it, is the difficulty of calibrating any particular model relating thermal data to soil moisture. The particular calibration will depend, in a very important way, on past weather history and present environmental conditions, including such things as wind speed and relative humidity. Therefore, without a great deal of ancillary data, thermal data will only be qualitatively relatable to soil moisture within a limited geographic region. In addition, use of albedo information is probably important for interpreting thermal relations to soil moisture, and we did not use such information.

Our data showing the relationship between scanner radiant temperature and soil moisture in partially vegetated terrain looks promising. This may be deceiving, however, in that all of the problems associated with bare soil areas are compounded in a vegetated canopy. However, the results furnish some basis for speculating that thermal data might be used to infer information concerning differential rates of evapotranspiration from vegetation canopies, and hence something

concerning soil moisture conditions within the root zone of the soil. Since the "target" is now the vegetation, rather than the soil, this could be done in canopies with essentially complete (100%) vegetation cover. Since we would like to know the moisture status below the surface, this particular possibility should be further investigated. Undoubtedly such a technique would require calibration to the "amount of transpiring area," such as appears to be possible using reflectance data.

Data from the literature shows that reflectance can be related to soil moisture. Such a relationship is dependent on the soil type, but it is not strongly dependent on past or present environmental conditions. Therefore, with adequate ancillary soils information, there appears to be hope of calibrating a soil moisture model and hence quantifying surface soil moisture of bare soil. The scanner data over bare soil areas which we processed are not inconsistent with this hope.

The additional, and perhaps greater, value of using reflectance data is its potential for estimating surface soil moisture in partially vegetated terrain. The reflectance modeling which was done suggests that this is a promising possibility, at least up to certain limiting values of percent vegetation cover. This limiting value can be extended to fairly high values of vegetation cover using near-zenith solar illumination or monostatic viewing/receiving as in a laser scanner.

One of the main limitations to using reflectance data is that subsurface soil moisture can not be directly measured. However, subsurface soil moisture might be inferred by using an evapotranspiration formula, with reflectance data forming the basis for a "vegetation factor."

Finally, it should be noted that thermal data and reflectance data used together will probably be more a more reliable indicator of soil moisture than either one independently. As a very limited test of

this assumption, field determined soil moisture was regressed against scanner IR reflectance data and IR/red reflectance ratio data, and then the scanner thermal data was added as an additional independent variable. The thermal data increased the significance of the regression equation. The challenge that remains is to learn how to interpret the thermal data under variable environmental and target conditions.

7

S192 DATA PROCESSING

7.1 S192 COVERAGE

Only one overpass of the designated test site for this project (the western Lake Ontario basin) occurred during the SKYLAB missions. This was SL3 Pass 29 (EREP Pass 40) on 9 September 1973. Unfortunately, a blinking alignment diode was inadvertently left on during the data collection and caused a "striping" effect to be present in all the reflective channel imagery (Figure 23). Without removal or at least alleviation of this striping effect, which was worst at short wavelengths, achieving useful results by computer processing was felt to be impossible. Processing of an alternative site was considered, but the only other SKYLAB overpass within the Lake Ontario basin, SL3 Pass 50 over the Finger Lakes area in New York state, had high cirrus cloud cover over some of the regions of principal interest. Consequently, it was decided that we would process the 9 September data, after first attempting to remove the alignment light striping effects.

7.2 DATA UTILIZED IN PROCESSING

We received two 9 track 800 bpi computer compatible tapes (CCTs) of the 9 September data. Only 8 of the possible 22 SDOs were made available to us: 5 and 6 (0.599-0.654 μm); 7 and 8 (0.654-0.734 μm); 9 and 10 (0.770-0.890 μm); and 16 and 21 (10.2-12.5 μm). The data extended from a GMT start time of 19:20:55.0169 to a GMT stop time of approximately 19:21:14.99 and were non-scan line straightened (conical) in format. In addition, we received screening films of SDOs 5, 7, 9, and 21.

FIGURE 23. S192 SCREENING FILM OF SDO 5 (0.599-0.654 μm) FOR SL3 PASS 29 OF 9 SEPTEMBER 1973. The area is southeastern Ontario Province, Canada and northern Lake Ontario. Note that the striping in the data, produced by a blinking alignment diode, crosses the scan lines at an angle.

7.2.1 DATA QUALITY

The on-off operation of the diode light resulted in a regular, nearly square wave of low frequency noise being added to the data. This pattern of regular increases and decreases in the baseline data values produced a striping of alternating light and dark bands across the scan lines. The striping appears to cross the scan lines at an angle because the square waves produced by the diode, which operated independently of the mirror rotation, are slightly offset in phase in successive scan lines.

The most severe striping effects were in SDOs 5 and 6, the red band. No effects were evident in the thermal SDOs. Figure 24 illustrates the condition of the data in SDOs 6, 10 and 16, prior to any attempts to remove the striping.

7.2.2 DATA PREPARATION

Modification of the S192 data to remove the low frequency waveforms introduced by the blinking diode was possible because our data was in conical format, and each scan line was arranged in its proper time sequence. Because of the regularity of the diode light waves superimposed on the data, it was decided to attempt to remove these striping effects by approximating the square wave with a sine wave and then subtracting the sine wave from the data. The first attempt, using an average period for the square wave of 265 pixels computed over all the data (1895 scan lines), did not produce uniformly good results because of apparent fluctuations in the scan rate throughout the data. Because of this variability, we decided to preprocess a subset of the data and use the period length determined by an average over just that region. The section of the data from the beginning to just beyond the Bowmanville, Wilmot, and Soper Representative basins was selected. This section of data contains 947 scan lines, or about half the

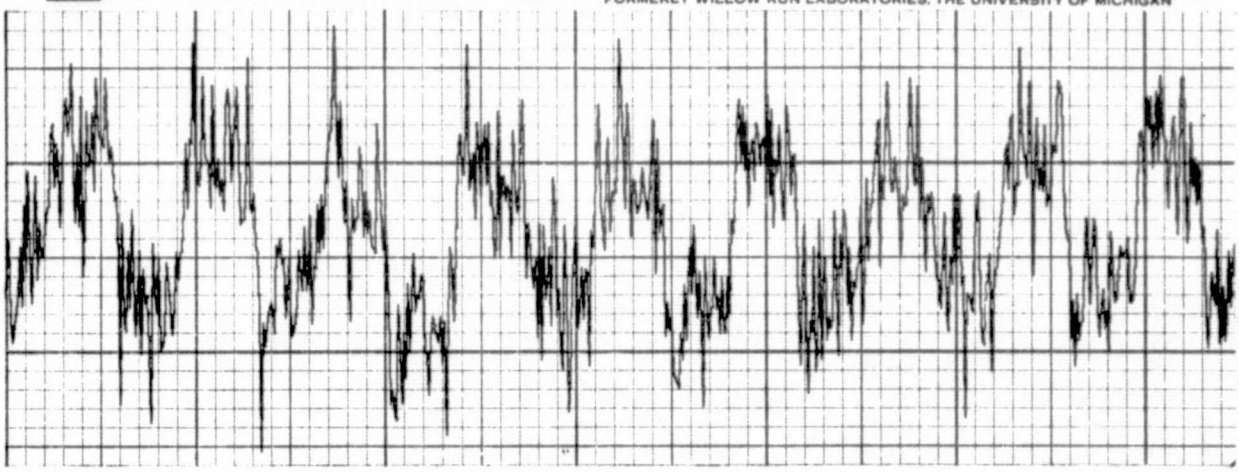

SDO 6 (.599-.654 μm)

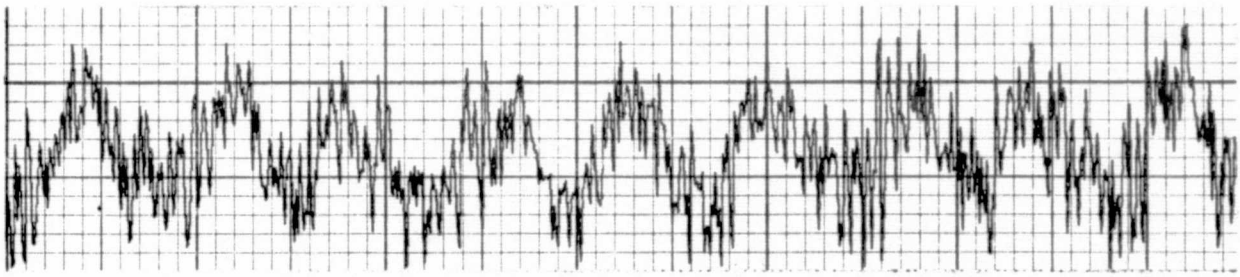

SDO 10 (.770-.890 μm)

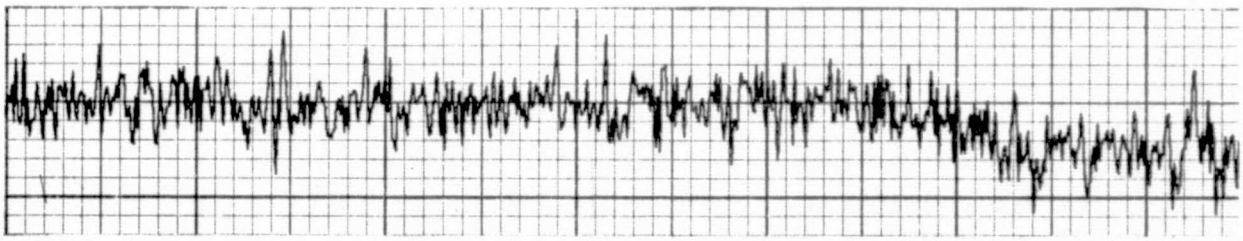

SDO 16 (10.2-12.5 μm)

FIGURE 24. TRACES OF SEVERAL SCAN LINES OF DATA IN SDO's 6, 10, AND 16 BEFORE DATA PREPARATION. Each trace represents an average of 16 adjacent pixels (21-36) plotted versus scan line number, from scanline 196 to 843. Note the regular wave pattern in SDO's 6 and 10. Scale is 10 digital counts per vertical inch for SDO's 6 and 10, 50 counts per inch for SDO 16.

original data. In addition, we decided to limit the number of SDOs on which data preparation was done because of cost considerations. SDOs 6 (0.599-0.654 μm) and 10 (0.770-0.890 μm) were selected for several reasons, including the fact that they approximated the red and near IR bandwidths used in the aircraft processing. SDOs 7 and 8 (0.654-0.734 μm), on the other hand, are intermediate between the red and the near IR regions and were not felt to be very useful for this project. In addition, choice of both SDOs as even (or odd) was necessary in order that the sampling method be the same for both channels so that problems with misregistration could be avoided.

Preparation of the data using the period length of 274 pixels determined over the reduced subset of data produced good results. Figure 25 illustrates SDOs 6 and 10 after subtraction of the sine wave. Since SDO 16 had no alignment light effects, it was merely copied onto the output tape with the corrected SDOs 6 and 10.

An indication of the magnitude of the effect of the low frequency noise produced by the alignment light on the data can be obtained by determining the average amplitude of the data over the period of the square wave before and after the sine wave subtraction. In SDO 6, the average amplitude went from approximately 4.1 counts to .94 counts; in SDO 10, it went from 2.5 counts to 1.25 counts. Figure 26 illustrates the effect of the alignment light on the data along one scan line. The before and after data preparation traces give an indication of how difficult it would have been to have obtained useful results processing the data without first removing the low frequency noise induced by the alignment light.

Even after removal of the noise produced by the alignment light, there was still considerable noise in the data. The high frequency noise present in the data is evident in all the traces (Figures 24-26) but is especially noticeable in the after data preparation traces over water.

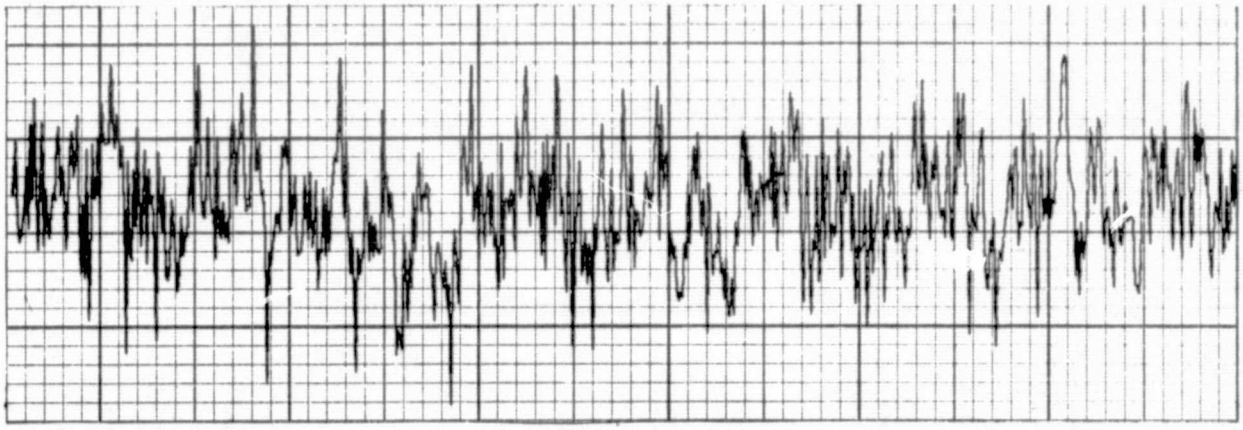

SDO 6 (.599-.654 μm)

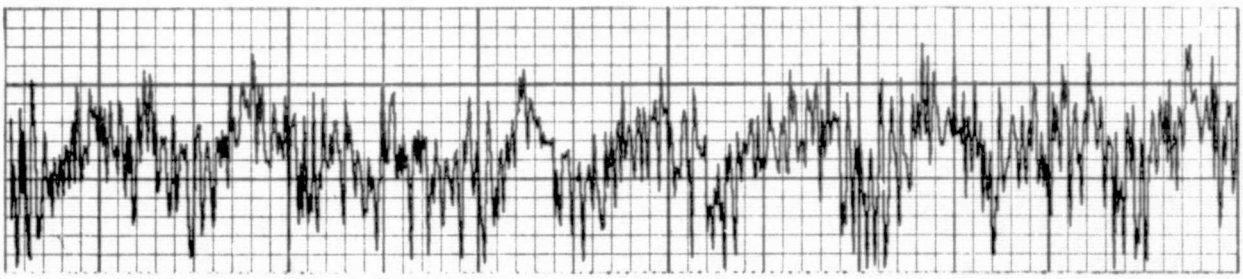

SDO 10 (.777-.890 μm)

FIGURE 25. TRACES OF SEVERAL SCAN LINES OF DATA IN SDO's 6 AND 10 AFTER DATA PREPARATION (subtraction of sine wave). Each trace represents an average of 16 adjacent pixels (21-36) plotted versus scan line number from line 196 to 843. Compare with Figure 24. Scale is 10 counts per vertical inch.

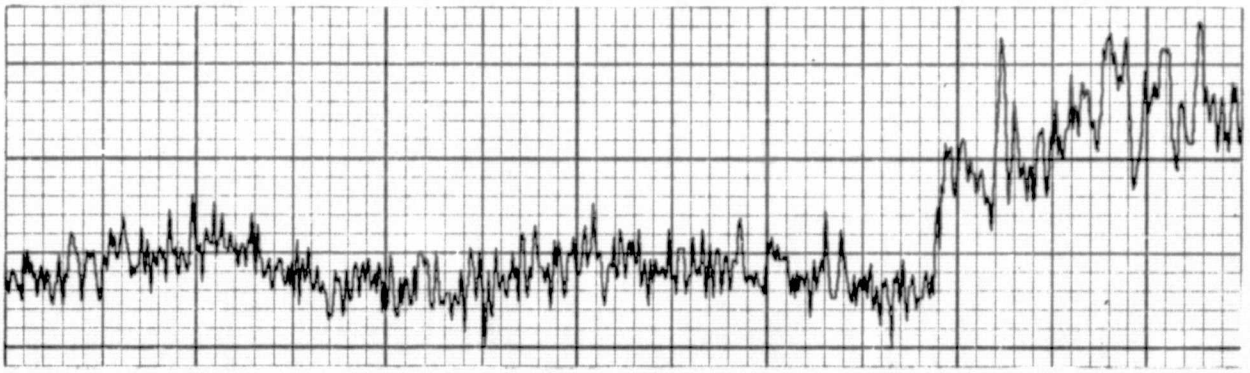

Line 97 SDO 6 (.599-.654 μm) Before Sine Wave Subtraction

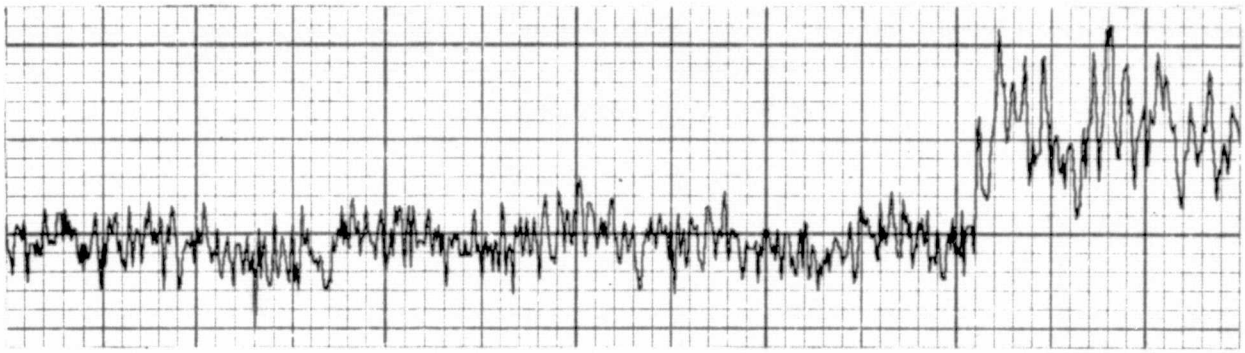

Line 196 SDO 6 (.599-.654 μm) After Sine Wave Subtraction

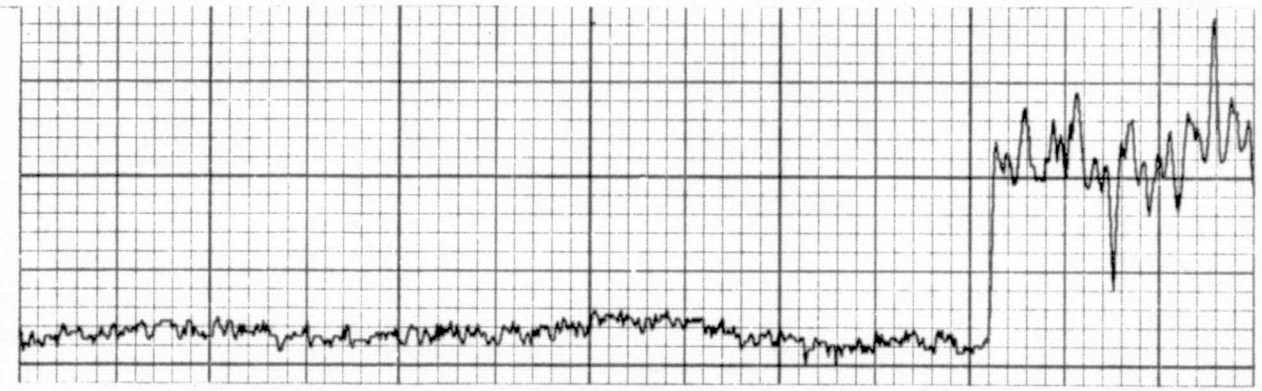

Line 196 SDO 10 (.770-.890 μm) After Sine Wave Subtraction

FIGURE 26. TRACES OF ONE SCAN LINE IN SDO's 6 AND 10 BEFORE AND AFTER DATA PREPARATION. Scale is 50 counts per vertical inch.

7.3 PROCESSING PROCEDURE

The initial step in the processing of the S192 data was generation of a 3 x 3 (every third line, every third pixel) graymap of SDO 6, the red band. This was done for orientation purposes and an initial evaluation of data quality.

Traces of both individual scan lines and averages of several pixels over many scan lines (Figures 25 and 26) had indicated considerable improvement in the overall data quality as a result of the data preparation. However, where the introduced sine wave crossed the side of the square wave no smoothing of signal value was achieved and a sharp spike in amplitude remained. This spiking of signal amplitude at the edges of the original squares waves was evident on the 3 x 3 graymap. Edges of "stripes" could be seen. This phenomenon was only a few pixels wide and the potential effect on computer recognition processing could not be evaluated.

In an effort to determine the extent of high frequency noise in the data the standard deviation over three large areas in Lake Ontario, each of apparently uniform reflectance and temperature, was computed. Table 7 lists the standard deviation obtained for each of the three areas in each of the SDOs we had available. This value can be taken as a measure of the random noise in the data if the underlying assumption of uniformity over the area computed holds true. The large standard deviation obtained for the third area in SDO 16 indicates less uniformity for this area than for the other two areas. Consequently, it was not used to compute the average standard deviation in SDO 16.

A measure of data quality which we have called the "signal-to-noise ratio" is also listed in Table 7. It was obtained by dividing the dynamic range of each SDO by the average standard deviation within that SDO. The dynamic range was defined as being 95% of the data value range (in counts) in each SDO from a sample of 152,121

TABLE 7

DYNAMIC RANGE, STANDARD DEVIATION, AND SIGNAL-TO-NOISE IN SDOs 6, 10, and 16

SDO	λ(μm)	Dynamic Range (Counts)	Standard Deviation (Counts)		Signal To Noise[4]
6	.599-.654	41	6.15[1]		6.61
			6.29[2]	Average: 6.20	
			6.17[3]		
10	.770-.890	38	2.93[1]		12.30
			3.17[2]	Average: 3.09	
			3.18[3]		
16	10.2-12.5	58	8.36[1]		6.63
			9.14[2]	Average: 8.75	
			11.27[3]		

[1]Computed over an area of 46,155 pixels
[2]Computed over an area of 50,680 pixels
[3]Computed over an area of 97,718 pixels
[4]dynamic range/average standard deviation ≡ signal to noise ratio

pixels over land (every line and every point over an area centered on the Bowmanville, Wilmot, and Soper basins). While the signal-to-noise ratios for SDOs 6 and 16 are nearly the same, that of SDO 10 is considerably greater.

7.3.1 WATER PROCESSING

The area in Lake Ontario covered by our S192 data is the most stable area, with the least current movement, in the lake. This condition is evident in Figure 7 which indicates the current patterns in the lake by the pattern of suspended solids. Virtually no variability was evident in the portion of Lake Ontario contained on the S192 screening film provided us for the red and near IR bands. While tonal differences were present on the thermal imagery, they mainly consisted of three broad areas of light, medium, and dark tones.

The standard deviations given in Table 7 were based on signatures from areas selected on the basis of differences in the thermal imagery. The means and standard deviations of the three signatures (from the light, medium, and dark toned areas) overlapped considerably in the red and near IR SDOs, 6 and 10. In addition, the middle and coldest temperature areas were not separable in the thermal SDO on the basis of signatures because of the large standard deviations. Therefore, we decided it would not be fruitful to process the available data over Lake Ontario for differentiation of water masses.

7.3.2 LAND PROCESSING

The main objective of the digital processing of the S192 data over land was to discriminate conditions (land uses) of hydrologic importance and map them. Previous processing of LANDSAT-1 data over the East and Middle Oakville Creeks basin [3]

and Bowmanville, Wilmot, and Soper Creeks basins [15] had identified hydrologically important land use categories identifiable using LANDSAT satellite data. Since the S192 data was centered on the Bowmanville, Wilmot, and Soper Creeks basins it was decided to use generally the same categories for the recognition processing of the S192 data that had been used for the LANDSAT-1 processing of the area.

A 1 x 1 graymap of voltage levels in SDO 6 was generated and examined. Because of the geometric distortion produced when conical data are printed in linear format, we did not feel that training sets for all the various categories could be manually chosen from the graymap with the necessary degree of accuracy. Consequently, six polygons were delineated based on the aircraft imagery obtained the day following the S192 data acquisition to encompass all major categories in the scene. An unsupervised clustering algorithm was then used with these six polygons (5778 pixels) to produce signatures.

Clustering produced 29 clusters with greater than 10 pixels. The class or classes predominantly recognized by each cluster signature was determined using maps of the polygons which labeled each pixel with its cluster assignment, in conjunction with the aircraft photography. In addition, the distribution of each cluster in a two channel scatterplot was examined. The distribution of each of the 29 clusters with more than 10 data points was represented as an ellipse whose boundary was a constant probability of one χ^2 distance from the mean. A comparison with similar ellipse plots of the LANDSAT-1 data from this area obtained late August the previous year gave additional information about the likely class represented by each cluster.

A recognition map of a test area was subsequently generated using selected cluster signatures. The additional information contained in this recognition map made location of specific areas

easier than on the single channel level slice map. Classification results were analyzed using the aircraft imagery. While certain classes were well recognized, others were not. Using the recognition map we attempted to manually define training sets for all categories that were not being well recognized. We also eliminated cluster signatures which were recognizing several different classes. Unit contour ellipse plots were generated using these training set signatures. As before, the ellipses were generated in all possible combinations of two channels: red versus IR, thermal versus IR, and red versus thermal.

Classification was again done over the test area, this time using both cluster derived and training set derived signatures. The recognition map was compared with the aircraft data and evaluated. In addition to this procedure, signatures were also evaluated using a program which computed the probability that pixels from a given signature distribution would be classified into each recognition class. Since the decision rules for computing this expected-performance matrix were the same as those used in the classification algorithm, this program gave a good insight into how well the various classes could be separated.

As expected from experience with the LANDSAT-1 data over Bowmanville, it was not possible to discriminate certain classes. Pine, for example, the signature of which had fallen entirely within a marsh signature ellipse in the LANDSAT-1 data set, was again recognized by a marsh signature in the S192 data set. The September data made discrimination of some of the vegetation classes impossible. Certain herbaceous vegetation classes looked like hardwoods, for example. Orchards as a class could not be discriminated from other types of vegetation, particularly hardwoods, because of the variety of differences in crown closure and the inherent similarity. Therefore, the orchard class was lumped into the hardwood class. Because

of such situations, the classes to be recognized were modified somewhat from those used in the LANDSAT-1 processing of this area.

The final classification was performed using 30 signatures to recognize 8 classes. Water was recognized using both a signature (from Lake Ontario) and a level slice in the near IR channel. A module, SPEC., was subsequently implemented. It reclassified all pixels initially recognized as upland herbaceous vegetation and some pixels recognized as bare soil into four levels of percent green vegetation cover and bare soil using appropriate values of a 10/6 SDO ratio as determined from analysis of the aircraft photography. The final classification map is shown in Figure 27.

7.4 ACCURACY ASSESSMENT

Determining the classification accuracy of the final map is an extremely difficult procedure. Most of the features in the scene are small in size and have irregular boundaries, so it is difficult to determine how individual pixels should be classified. This problem is seriously compounded by the fact that the data is not scan-line straightened, which makes it nearly impossible to locate the true location of individual pixels with accuracy. As a result of the foregoing problems it was decided to assess the potential accuracy of the classification based on the statistics of the input signatures, using a program called PEC.

PEC. uses the input sigantures to generate 1000 points for each signature, with the points generated having a normal distribution. The 1000 points are then classified using the best linear classification rule. The resulting allocation of the points to the various classes is the basis for computation of the classification accuracy. (Table 8) Since this accuracy figure is based on idealized training set data, it represents the best classification one could obtain if the real data had the same characteristics. In most situations this will probably not be the case, so actual classification accuracies will generally

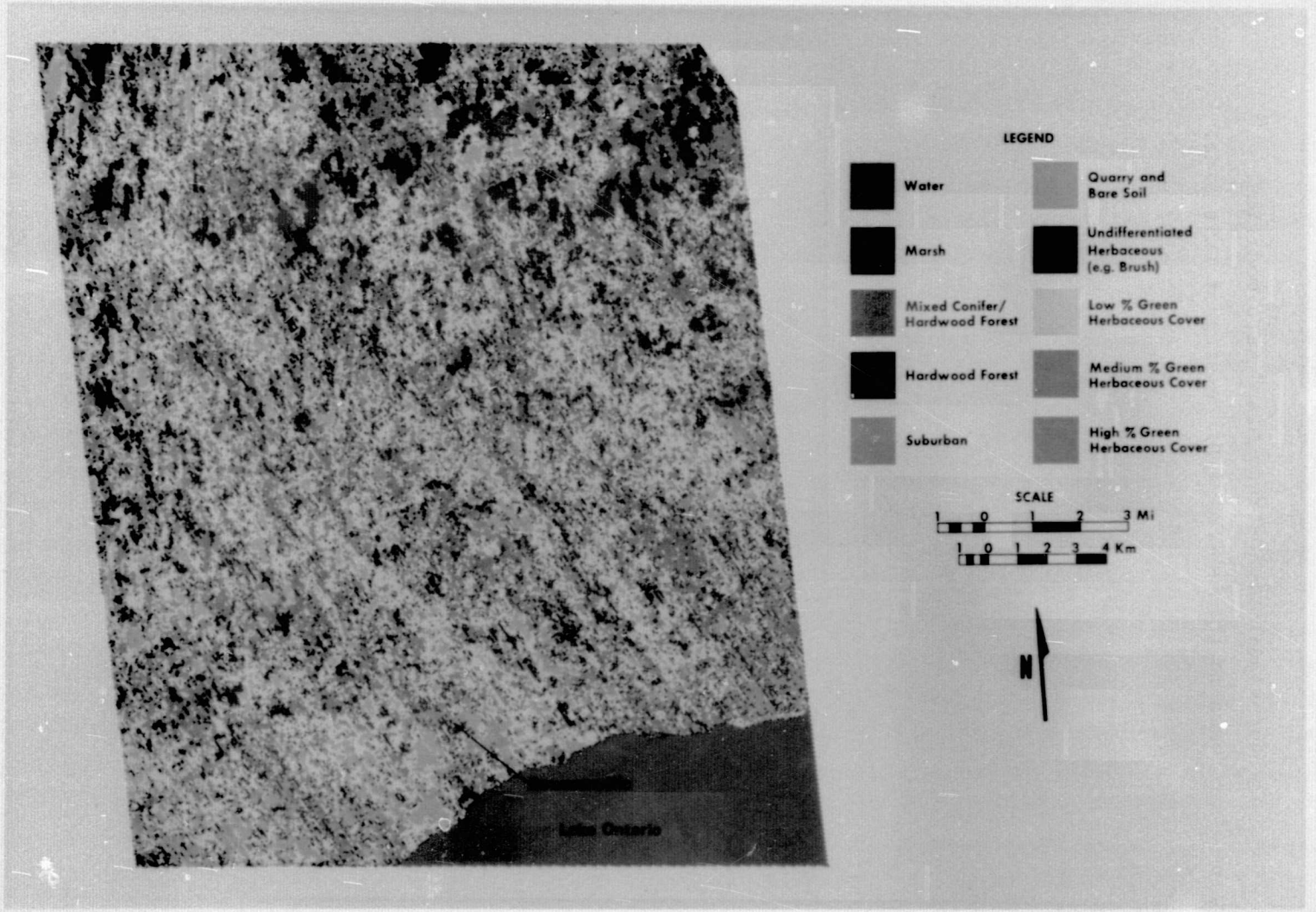

FIGURE 27. SKYLAB S192 RECOGNITION MAP. Color coded ink jet display of the final classification map of an area of approximately 1241 km^2 (479 mi^2) in southeastern Ontario, Canada centered at 43^{o}9'N/78^{o}41'W. The map was generated from Skylab S192 data obtained 9 September 1973 during SL3 Pass 29. The data used were non scan line corrected, which accounts for the skew apparent in the map. The arrow indicates north at the center of the scene. Scale, because of the distortion, is approximate.

TABLE 8

PROBABILITY OF CORRECT CLASSIFICATION OF THE EIGHT CATEGORIES MAPPED BASED ON ANALYSIS OF SIGNATURES USING PEC

Class	% Correct
Marsh	.9735
Conifer/Hardwood	.9055
Hardwood/Orchard	.9470
Undifferentiated Vegetation (brush, idle, etc.)	.7889
Suburban	.7765
Bare Soil/Quarry	.9530
Herbaceous Vegetation	.9386
Water	.9900

lower than these. However, it is possible to obtain insight as to which signatures (classes) are likely to be confused with each other. Probabilities of misclassification were generally low and are not listed in Table 8. All categories except two had probabilities of correct classification above 90% with the average of these near 95%. The two other classes fell in the 78 to 79% correct classification range. The suburban and brush categories had the lowest probability of correct classification, and the greatest misclassification occurred between these two categories. 27.5% of the suburban class was called suburban. In addition, 9.4% of the suburban class was misclassified as bare soil. It is not surprising that the suburban category was subject to misclassification into a vegetation and soil class, since the suburban class is, in fact, a mixture of those and spectrally similar classes.

7.5 COMPARISON OF CLASSIFICATION USING SKYLAB AND LANDSAT DATA

The same general area that was classified using SKYLAB data had been previously classified into approximately the same classes using LANDSAT data which was collected approximately one year before the SKYLAB data [15]. A map of the LANDSAT classification is shown in Figure 28. The percentage of the land area recognized as various classes using SKYLAB and LANDSAT data sets is given in Table 9.

It can be seen that the percentages of the area recognized as mixed conifer/hardwood and as bare soil (including gravel quarries) are approximately the same for the two data sets. The total percentage area recognized as green herbaceous cover is also quite similar on the two data sets, being 52.82% on LANDSAT data and 52.66% on S192 data. The three categories for which there is reasonably good agreement comprise a total of approximately 3/4 of the total area.

There is less good agreement between LANDSAT and SKYLAB results for the remaining categories. There is a large discrepancy in the percentage of the area classified as hardwoods. Our analysis of the

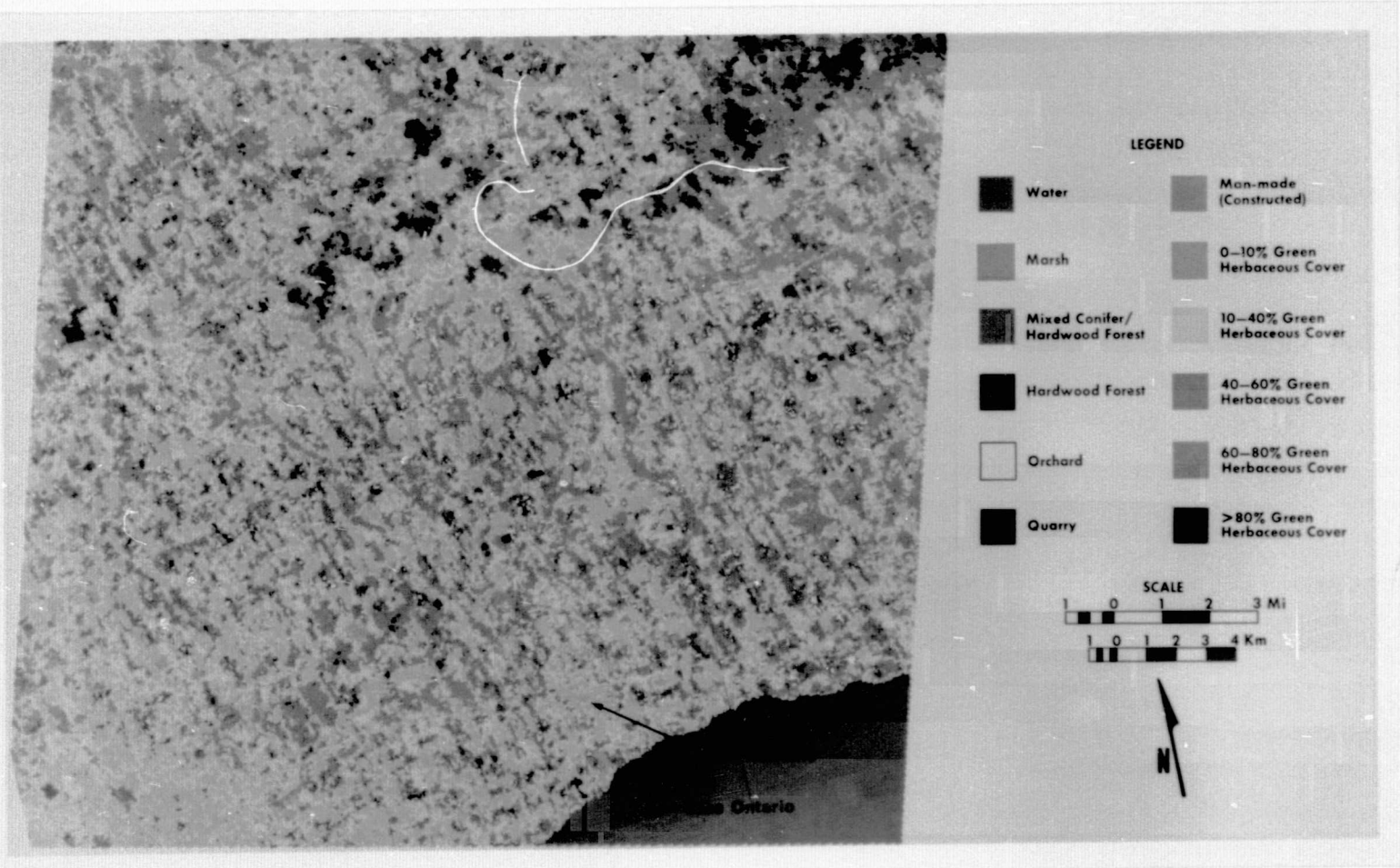

FIGURE 28. LANDSAT RECOGNITION MAP. Color coded ink jet display of the final classification map of an area of approximately 1231 km^2 (475 mi^2) in southeastern Ontario, Canada centered at 44°00'N/78°42'W. The map was generated from LANDSAT-1 data obtained 20 August 1972 (scene 1028-15290). The data have been geometrically corrected.

TABLE 9

COMPARISON OF LANDSAT AND SKYLAB RECOGNITION OVER AN AREA CONTAINING THE BOWMANVILLE, WILMOT, AND SOPER REPRESENTATIVE BASINS

CLASS	PERCENT OF TOTAL LAND CLASSES (LANDSAT)		(S192)
Marsh	3.15		1.63
Mixed Conifer/Hardwoods	15.35		13.69
Hardwoods	3.97[1]		11.91
Bare Soil and Gravel Quarries	8.37		7.41
Man-Made	15.94		----
Suburban	----		8.40
10-40% Green Cover	25.43		----
Low % Green Cover	----		27.72
40-60%	13.20	25.18	----
60-80%	11.98		----
Medium % Green Cover	----		22.76
80-100%	2.21		----
High % Green Cover	----		2.18
Brush	----		4.30
Unclassified	.41		----
TOTAL	100.005		100.01

[1]Includes 1.025% Orchard Class

classification based on aerial photography suggests that too much of the SKYLAB data was classified as hardwoods whereas too little of the LANDSAT data was classified as hardwoods. For the most part, this overrecognition in the S192 data seems due to certain agricultural crops being classified as hardwoods and to a larger proportion of the mixed conifer/hardwood forest being classed as hardwoods in the SKYLAB data than in the LANDSAT data. We feel that much of this difference in percent of hardwoods recognized is due to differences in signatures used in the recognition and to seasonal differences in the vegetation rather than to differences in the data quality.

Some of the same difficulties in the marsh recognition were encountered in both data sets (e.g., the impossibility of separating pine from marsh mentioned previously). In general, however, there appeared to be more misrecognition, primarily upland herbaceous vegetation as marsh, with the LANDSAT data than with the S192 data. In the SKYLAB processing, though,considerable misrecognition of marsh occurred along the shoreline, suggesting a situation of mixture pixels. Finally, some marsh areas in the S192 data were classified as water.

The most severe misclassification in the LANDSAT data occurred in the man made category. Overrecognition occurred and in general the confusion was with bare soil. The equivalent category in the S192 processing, suburbs, was also confused in some cases with bare soil but not nearly so much as in the LANDSAT data. Not all of the suburban areas were recognized in the SKYLAB data nor were roads as well recognized as they were on the LANDSAT data. but overall the percentage of the scene occupied by that class is felt to be more nearly correct on the SKYLAB data. Some undifferentiated vegetation areas were recognized as suburb in the S192 data.

Another area of difference in classification occurred with inland water bodies. The LANDSAT classification was very good at

recognizing small waterbodies. The SKYLAB classification, on the other hand, recognized very few of the waterbodies, even those of several acres in size. Furthermore, some marsh areas were recognized as water on the SKYLAB data.

In conclusion, it appears as though the S192 and LANDSAT data are reasonably equivalent in terms of their information content and their ability to recognize the classes in this scene. Most of the difference in the percentage of the area recognized as particular classes can be accounted for by differences in the training set signatures used, rather than any fundamental difference in information content.

7.6 IMPORTANCE OF THERMAL BAND

The main difference between LANDSAT data and the SKYLAB data we processed (in terms of the spectral information available) was the existence of a thermal channel on the SKYLAB data. Accordingly we tried to assess the importance of the thermal information. Unfortunately, it is difficult to assess the importance of the thermal band from the data which have been processed. Only three spectral bands were used in processing, and many investigations have shown improvements in classification by addition of a third spectral band, regardless of the wavelength. Therefore, a comparison of classification accuracy with and without the thermal band is probably not very meaningful, and was not attempted.

In addition, the noise problem which affected the red and near IR bands did not affect the thermal band, so the inherent relative value of the thermal information, per se, is difficult to assess.

The distribution of the clusters which were formed by the clustering program were analyzed to determine if thermal data was providing unique information. Two clusters occurred at nearly the same spot on a plot of red and near IR reflectance, and were in the

region where it was presumed they were both green herbaceous vegetation. However, in the thermal channel one cluster had a mean value of 178 (digital counts) and the other cluster had a mean value of 115 (digital counts). One possible interpretation of this situation is that the thermal band is furnishing unique and valuable information. One cluster might be a vegetation canopy with very moist soil and the other cluster a vegetation canopy with very dry soil. However, 178 is the highest mean value of all clusters in the thermal band. It seems unlikely that any vegetation canopy would have that characteristic, no matter how dry the soil.

In conclusion, therefore, we do not feel we can make any definitive statements about the usefulness of thermal information for recognizing the classes of interest in this investigation.

8

SUMMARY, CONCLUSIONS, AND RECOMMENDATIONS

The purpose of this research was to assess hydrological conditions of selected portions of the Lake Ontario drainage basin. Aircraft scanner data and Skylab S190A, S190B, and S192 data were all analyzed.

The S190A and S190B photography proved to be useful for mapping large scale geomorphological features, and for assessing water depth and water quality. The greater spectral resolution in the S190A photography and the greater spatial resolution in the S190B photography both had advantages for identifying certain features.

The available S192 data was affected by low frequency noise caused by a diode light, but data preparation was successful in partially reducing this problem. Computer processing was implemented on a red (channel 6), near IR (channel 10), and thermal (channel 16) band. Features of hydrological interest were classified, and upland green herbaceous vegetation was separated into several classes on the basis of percent vegetation cover. It was not possible to make accurate quantitative determinations of classification accuracy, but comparison with processed LANDSAT data over the same area indicated that recognition accuracies were roughly equivalent. The importance of the information in the S192 thermal band could not be determined.

A model for estimating surface soil moisture based on red and near infrared reflectance data was developed and subsequently implemented on aircraft scanner data. The lack of S192 data over the specific test site where both ground and aircraft data were obtained precluded us from extrapolating these results to space data. However, the promising results using aircraft data suggest that the technique should be further developed using space acquired data. More attention should also be given to theoretical modeling such as was used in this investigation in order to gain insight into the optimum spectral bands and signal-to-noise requirements for further space sensor systems.

APPENDIX

LISTING OF SMOIST. PROGRAM FOR CALCULATING SOIL MOISTURE

```
$COMPILE MAC

AC (09 AUG 1965 VERSION) PROGRAM LISTING ... ... ...


              EXTERNAL FUNCTION SMOIST.
             *
             ************************************
             * CALCULATES THE PERCENT MOISTURE IN SOIL, GIVEN AN I.R.
             * CHANNEL, AN IR/RED RATIO CHANNEL AND 5 COEFICIENTS
             *
             * A,B,C,D,E  COEFICIENTS    (DEFAULT=0.)
             * IR  IR CHANNEL (REFLECTANCE)  (DEFAULT = 1)
             * RAT RATIO CHANNEL (REFLECTANCE) (ASSUMES RATIO=VALUE/100)
             *                               (DEFAULT = 2)
             * OC  CHANNEL IN WHICH TO WRITE ANSWERS    (DEFAULT = 1)
             * NC  NUMBER OF OUTPUT CHANNELS   (DEFAULT = 1)
             * SMR SMOIST RECTANGLE FOR PRINTING RESULTS
             *                 (DEFAULT = NO PRINTER OUTPUT)
             *
             ************************************
             *
              NORMAL MODE IS INTEGER
              REFERENCES ON
              ERASABLE SKP2(225), CUNIT, CREEL, CFILE, CLINE, TWRITE, CCHAN,
             1   CNWDS, PROG, MODE1, MODE2, UNIT, CALINE, CCLINE, NSA, NSP,
             2   KS, NA, NB, KP, ID(1), TFLAG, IPACK, RESERV(4), CFACTR(49),
             3   CTITL2(19), CTITLE(19), CLIST(19), CSPARE(46), CFLAG,
             4   CBANG, CBANG, CKP, CNA, CNSS, CNCHAN, CMODE, CRECA, CRECC,
             5   CFILE, CREEL, CNWDS
              ERASABLE DATA(423), ITEST, OSTART, CSTART, NV, NX, NC, L, IF,
             1   IOP, NOP, NEXT, START2, READT2, READL2, READF2, LABEL2,
             2   EXTRA(20), DATUM(24), ICODE(24), ICHAN(24)
              FLOATING POINT CFACTR(49),SCALE
              EQUIVALENCE (NCH,DUM(191)),(FDUM,DUM)
              EQUIVALENCE (DUM(28),CFACTR)
              FLOATING POINT A,B,C,D,E,RAT2,VAL,IR2,ACC,MULT,T,VAL2
              FLOATING POINT TT(511)
              VECTOR VALUES PFLAG=C
              DIMENSION SMR(10)
              BOOLEAN PF
              WHENEVER NEXT.G.5, FUNCTION RETURN
              TRANSFER TO STEP(NEXT)
             *
             ***************
 STEP(1)      PRINT COMMENT $1 SMOIST. (VERSION 1.0)  9/744
             *
             *   PRINT OUT TABLES FOR INTEGER LEVELS VS. PERCENT
             *      PRINT TABLE FIRST TIME THROUGH ONLY
              WHENEVER PFLAG.E.C
                THROUGH PL1,FOR I=1,1,I.G.511
 PL1          TT(I) = (I-1)/5.1CCC1
              PRINT FORMAT $H'- PERCENT VS INTEGER LEVEL',/
             1   /(S1,(6(I3,S2,F7.2,H'  **  ')))*$,(I=1,1,I.G.511,I,TT(I))
              PFLAG=1
              END OF CONDITIONAL
             *
              SPRAY.(-1,SMR(C)...SMR(5))
```

```
            A=C.
            B=C.
            C=C.
            D=C.
            E=C.
            IR=1
            RAT=2
            CC=1
            NC=1
            SCALE=1.C
           *
            READ AND PRINT DATA A,B,C,D,E,IR,RAT,CC,NC,SCALE
           *
            LINK.(CALC.)
            FUNCTION RETURN
           *
           ***************
STEP(2)     ADD=-1./5.1CCC1
            MULT=1./5.1CCC1
           *
           * SET QFACTOR VALUES ON OUTPUT TAPE
            WHENEVER QFLAG.E. 1, TRANSFER TO GQ
            QFLAG=1
            (I=1,1,I.G.CCHAN,QFACTR(I)=1.,QFACTR(I+25)=0.)
GQ          QFACTR(CC)=MULT
            QFACTR(CC+25)=ADD
            PRINT FORMAT OUT1,IR,RAT,NC,CC
            VECTOR VALUES OUT1=$H'-     INPUT CHANNELS ',/,S10,
           1 H'I.R.          = CHANNEL ',I2/S10,H'(IR/RED)*10C = CHANNEL ',
           2   I2,/,H'C     NO. OF OUTPUT CHANNELS = ',I2,/,
           3   S5,H'CALC. PERCENT CHANNEL  = ',I2*$
            PRINT FORMAT OUT2,A,B,C,D,E
            VECTOR VALUES OUT2=$H'-     TRANSFORMATION USED ',/,S53,
           1   S14,H'2',S18,H'2',/,S9,F8.4,H'  +',F8.4,H'(IR)  +',
           2 F8.4,H'(IR/RED)   +',F8.4,H'(IR)   +',F8.4,H'(IR/RED)'*$
            PRINT COMMENT $-     LINE      POINT      IR      RAT      PERCENT
           1       SCALED$
            FUNCTION RETURN
           ***************
           *
           *   CALCULATE BEFORE SEE THE LINE IF SHOULD PRINT INFO FOR
           *   THIS LINE
STEP(3)     PF=CB
            WHENEVER SMR(C).L.0., FUNCTION RETURN
            WHENEVER CALINE.GE.SMR(C) .AND. CALINE.LE.SMR(1)
            DIF=CALINE - SMR(C)
            IDIF = DIF/SMR(2)*SMR(2)
            WHENEVER DIF.E.IDIF, PF=1B
            END OF CONDITIONAL
           *
           ***************
STEP(4)     FUNCTION RETURN
           ***************
STEP(5)     PRINT COMMENT $- SMDIST. COMPLETE FOR THIS RECTANGLE$
            FUNCTION RETURN
            VECTOR VALUES OUT=$S3,I6,S5,I5,F7.2,F8.2,S4,F7.2,S7,I4*$
           *
           ***************
            INTERNAL FUNCTION CALC.
            V=DATUM(RAT)
```

```
      VAL=V*C.1
      RAT2 = VAL*VAL
      VAL2 = DATUM(IR)*SCALE
      IR2 = VAL2*VAL2
      T = A + B*VAL2 + C*VAL + D*IR2 + E*RAT2
      DATUM(OC) = T*5.1CC1 + 1
      WHENEVER DATUM(CC).G.511,DATUM(CC)=511
      WHENEVER DATUM(CC).L.C, DATUM(CC)=C
      WHENEVER PF
      WHENEVER IP.L.SMR(3) .OR. IP.G.SMR(4), TRANSFER TO RET
      DIF = IP-SMR(3)
      IDIF=DIF/SMR(5)*SMR(5)
      WHENEVER DIF.NE.IDIF, TRANSFER TO RET
      PRINT FORMAT CUT, CALINE,IP,VAL2,VAL,T,DATUM(CC)
      END OF CONDITIONAL
RET   FUNCTION RETURN
      END OF FUNCTION
      END OF FUNCTION
```

REFERENCES

1. Graeme Bonham-Carter and John H. Thomas, "Numerical Calculation of Steady Wind-Driven Currents in Lake Ontario and the Rochester Embayment," Proceedings of the 16th Conference on Great Lakes Research, International Association for Great Lakes Research, Braun-Brumfield, Inc., Ann Arbor, Michigan, 1973, pp. 640-662.

2. T. J. Simons, "Development of Numerical Models of Lake Ontario: Park 2," Proceedings of the 15th Conference on Great Lakes Research, International Association for Great Lakes Research, Braun-Brumfield, Inc., Ann Arbor, Michigan, 1972, pp. 655-672.

3. T. W. Wagner and D. L. Rebel, "An ERTS-1 Investigation for Lake Ontario and its Basin," Report No. 193300-65-F, Environmental Research Institute of Michigan, Ann Arbor, Michigan, 1975.

4. R. K. Vincent, R. Horvath, F. Thomson, and E. A. Work, "Remote Sensing Data-Analysis Projects Associated with the NASA Earth Resources Spectral Information System," Report No. 3165-26-T, Environmental Research Institute of Michigan, Ann Arbor, Michigan, 1971.

5. V. L. Prentice, "Multispectral Remote Sensing Techniques Applied to Salinity and Drainage Problems in the Columbua Basin, Washington," Ph.D. Dissertation, The University of Michigan, University Microfilms, Ann Arbor, Michigan, Microfilm No. 73-11232, 1972.

6. M. B. Blanchard, R. Greeley, and R. Goettelman, "Use of Visible, Near-Infrared, and Thermal Infrared Remote Sensing to Study Soil Moisture," Proceedings of the Ninth International Symposium on Remote Sensing of Environment, 1974, Volume 3, pp. 693-700.

7. S. B. Idso, T. J. Schmugge, R. D. Jackson, and R. J. Reginato, "The Utility of Surface Temperature Measurements for the Remote Sensing of Surface Soil Water Status," Journal of Geophysical Research, 1975, Volume 80 #21.

8. H. D. Buckman and N. C. Brady, The Nature and Properties of Soils, Macmillan Co., New York, 1969.

9. W. R. Van Wijk (ed), Physics of Plant Environment, North-Holland Publishing Company, Amsterdam, 1963.

10. E. H. Stockhoff, R. T. Frost, and E. J. Buerger, "Remote Soil Measurements," General Electric, Final Report, Prepared for NASA/GSFC on Contract NAS5-21689, 1973.

11. J. E. Colwell, "Bidirectional Spectral Reflectance of Grass Canopies for Determination of Above Ground Standing Biomass," Ph.D. Dissertation, The University of Michigan, University Microfilms, Ann Arbor, Michigan, Microfilm No. 74-15693, 1973.

12. S. A. Bowers and R. J. Hanks, "Reflection of Radiant Energy from Soils," Soil Science, 1965, Volume 100 #2, p. 130.

13. H. R. Condit, "The Spectral Reflectance of American Soils," Photogrammetric Engineering, 1970, Volume 36 #9, p. 955.

14. G. Suits, "The Calculation of the Directional Reflectance of a Vegetative Canopy," Remote Sensing of Environment, 1972, pp. 117-125.

15. D. L. Rebel, "Hydrological Land Use Classification of the Bowmanville, Soper, and Wilmot River Basins in Ontario, Canada Using LANDSAT-1 Data," Report No. 500600-1-F, Environmental Research Institute of Michigan, Ann Arbor, Michigan, 1976.

16. Earth Observations Aircraft Program Mission Report, Mission 85M, NASA Project S427, Environmental Research Institute of Michigan, Ann Arbor, Michigan, October 1973.